Data Report on Mapping the Hydrogeology near the City of Madison, Nebraska Using an Airborne Electromagnetic Survey

Clint P. Carney P.G.
Jared D. Abraham
James C. Cannia P.G.

Prepared for the City of Madison, Nebraska



EXPLORATION RESOURCES INTERNATIONAL

January 27, 2014

Data Report on Mapping the Hydrogeology near the City of Madison, Nebraska Using an Airborne Electromagnetic Survey

Prepared for:
The City of Madison
211 S Lincoln St
Madison, NE 68748

Submitted by:
Exploration Resources International Geophysics, LLC
6207 Hwy 80 East
Vicksburg, MS 39180
Phone: (866) 974-6867

Clint P. Carney, P.G.
Clint.Carney@xrigeo.com

Jared D. Abraham
Jared.Abraham@xrigeo.com

James C. Cannia, P.G.
Jim.Cannia@xrigeo.com



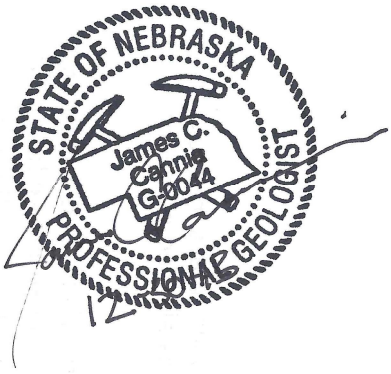


Table of Contents

Executive Summary **1**

Introduction **2**
Purpose and Scope **2**
Description of the Project Area **2**

Airborne Electromagnetic Survey **3**
Method **3**
AEM Measurements **4**
AEM Data Processing **6**
Automatic Processing 6
Manual Processing and Laterally Constrained Inversions 6
Spatially Constrained Inversion 7
Data Display and Interpretation 7

Hydrogeology of the Project Area **8**
Geologic Setting **8**
Hydrogeology of Quaternary Deposits 9
Cretaceous Geology and Aquifer Potential 10
Interpretation of AEM Results **11**
Map of the Principal Aquifer 11
Estimate of Aquifer Volume 12
Relationship to Current Test Holes and Production Groundwater Wells 13
Estimated Potential Recharge Areas 14

Summary and Recommendations **14**

Bibliography **16**

Appendix 1- AEM Interpretive Imagery **20**

Appendix 2 - Metadata **39**

Appendix 3 - Ancillary Data **43**

List of Figures

Figure 1 – Madison Project Area. **3**
Figure 2 – Flight line locations over the Project Area. **5**
Figure 3 – Locations of registered wells by use and CSD test holes in the Project Area. **10**
Figure 4 – Comparison of the subsurface resistivity (scale on the left) and the lithologic classifications at two borehole log locations. **13**

Length and Flow Rate Conversion Factors

Multiply	By	To Obtain
	Length	
kilometers	0.62	miles
meters	3.28	feet
millimeters	0.039	inches
	Flow Rate	
cubic meters/minute	264.2	gallons/minute
cubic meters/minute	0.59	cubic feet/second

Executive Summary

Exploration Resources International (XRI) is pleased to submit our report to the City of Madison titled ñData Report on Mapping the Hydrogeology near the City of Madison, Nebraska using an Airborne Electromagnetic Survey.ò This project began in August 2013 to address the water resource concerns of the city of Madison and in the immediate surrounding area. This area is of great interest to town because of the potential for development of new wells that may affect the current water supply for the city. XRI entered into an agreement with the city of Madison to undertake a hydrogeologic study of the area.

The scope of work for this project is as follows:

> An Airborne Electromagnetic (AEM) survey will be flown over a specified area near the city of Madison to support creation of the hydrogeological framework of this area. This framework will be provided as preliminary AEM data and as a final product in a data report. The AEM survey will be flown at approximately 300 meter spacing in a north-south direction and approximately 1500 meter spacing in an east-west direction. Approximately 75 kilometers of AEM survey will be flown.
>
> A. The Contractor shall acquire an AEM survey flown over the city of Madison to provide the hydrogeological framework, commencing on or around August 9, 2013. Status reports of the flying will be provided to the Client daily, including the areas flown, production rates, and flight plan for the following day.
>
> B. The Contractor shall process and quality assure/quality control all of the data collected from the AEM and ground system.
>
> C. The Contractor shall invert the AEM data and then derive a 3D electrical model of the surveyed area. These inverted, georeferenced data will be delivered to the Client.
>
> D. The Contractor shall provide a hydrogeologic framework report that will include maps of aquifer(s), estimate of aquifer(s) volume, map of aquifer(s) relationship to current test holes and production groundwater wells, and a map of estimated potential recharge areas. The report will also include all data and metadata files. The report will be delivered in PDF digital format.

Introduction

Purpose and Scope

Future water management decisions for the city of Madison have increased the need for detailed hydrogeologic frameworks for the area around the city. Demand for increased groundwater development near the city for various uses has required the city to evaluate whether the current supply can be expanded without degradation to the existing wells. Recent drought conditions (2012) in the area have increased interest from other government entities to look for an additional groundwater supply. If new groundwater development is expanded into the area of the city wells, the city needs to understand the aquifer geometry, characteristics, connection with surface water, adjacent aquifers and water production wells. There are three (3) Conservation and Survey Division (CSD) test holes in or near the area. These test holes are vital to the understanding of the area, but they cannot provide enough information to complete a detailed hydrogeologic framework.

Therefore, it was recommended that airborne electromagnetic (AEM) surveys be performed to supplement the test hole information and in turn used to develop a new hydrogeologic framework. The detail in the new hydrogeologic framework gives greater confidence to regulators, investors, and the public in water management decisions and practices because the understanding of the natural system is represented in detail never before achieved. This information also allows for future exploration of undeveloped potential groundwater resources.

Historic and traditional geologic information must be part of any AEM study, and it was included in the hydrogeologic framework generated in this study. The hydrogeologic framework developed from the AEM data allows the user to visualize the subsurface in 3 dimensions and understand the relationship of the existing wells to the aquifer. It also allows the user to calculate volumes of aquifer materials and an estimate of groundwater in storage. The AEM survey provides nearly continuous data of the subsurface. It was acquired quickly without trespass onto private property and without any property damage.

Description of the Project Area

The project area (Figure 1) surrounds the city at a distance out to approximately 1 mile. The city lies within Madison County. This area is glaciated, and the topography and landforms of the area reflect this. The hydrogeology of the area is defined by this glacial history and will be discussed later in the report. Agriculture is the main economic activity of the area. Groundwater supply is limited to the coarse glacial sediment packages and alluvium that occupy a small percentage of the overall glacial sediment of the area. There are a few irrigation wells in the area, along with some domestic and municipal supply wells.

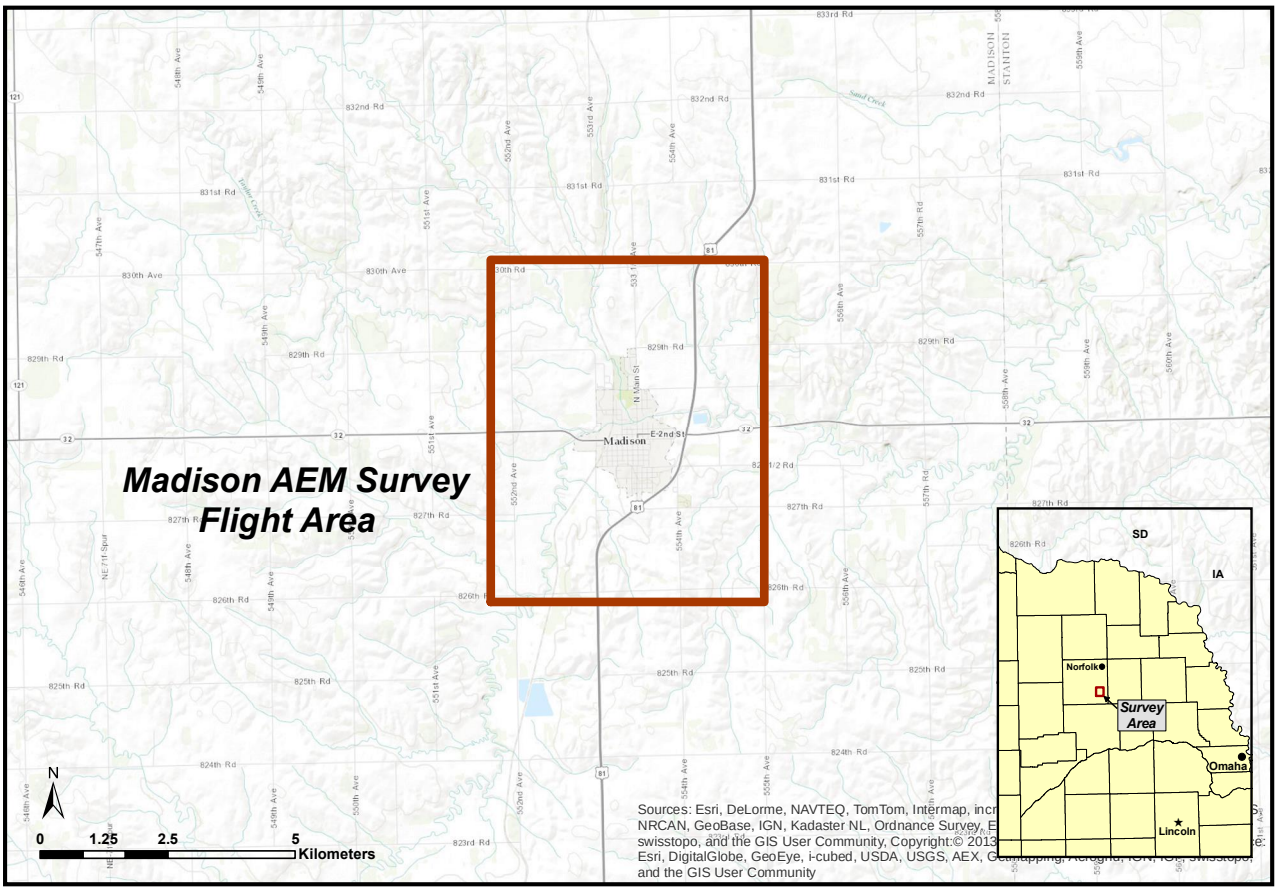


Figure 1 – Madison Project Area.

Airborne Electromagnetic Survey

Method

AEM surveys, flown with either helicopter or fixed-wing aircraft, increasingly have been employed to characterize aquifers and their geologic setting (Fitterman and Deszcz-Pan, 1998; Wynn, 2002; Jørgensen and others, 2003; Paine and Minty, 2005; Møller and others, 2009; Viezzoli and others, 2010; Abraham and others, 2011a; Abraham and others, 2011b; Jorgensen and others, 2012; Oldenborger and others, 2013; Lawrie and others, 2013). AEM surveys can provide characterization of electrical properties of earth materials from the near-surface 1 to 3 meters down to depths of 300 to 600 m. Typical AEM systems transmit an electromagnetic (radio-frequency) signal that interacts with the earth to generate (induce) secondary currents. Those secondary currents are a function of the subsurface electrical resistivity, which is controlled by the amount of mineralogical clay, gravel, water content (and the dissolved solids in the water), metallic mineralization, and void space. Measurements of the secondary currents are recorded either in the time domain (where the signal is a train of pulses and measurements are taken between the primary field pulses as a function of time as the secondary currents decay) or in the frequency domain (where the signal is a continuous wave and measurements are taken at the frequency of the primary

field, which is still present). Using numerical imaging and inversion, depth sections of estimated electrical resistivity can be created along flight lines. Interpolations between flight lines provide an estimation of the 3-D distribution of electrical resistivity and are presented as 3-D resistivity model.

Electromagnetic geophysical methods detect variations in the electrical properties of rocks ð in particular, electrical resistivity, or its inverse, electrical conductivity. Electrical resistivity can be correlated with geologic units on the surface and at depth using lithologic logs to provide a 3-D picture of subsurface geology. In the upper crust, the resistivities of geologic units are largely dependent upon their fluid content, pore-volume porosity, effective porosity, and conductive mineral content (Keller, 1989). While there is not a one-to-one relationship between lithology and resistivity, there are general correlations that can be made using typical values, even though values can be found at other localities that may fall outside of the ranges presented herein (Palacky, 1987). Fluids within the pore spaces and fracture openings can reduce electrical resistivities in what would otherwise be a resistive rock matrix, especially if the fluids are high in total-dissolved solids. Resistivity can also be lowered by the presence of electrically conductive clay minerals, graphitic carbon, and metallic mineralization. For example, it is common for altered volcanic rocks to contain replacement minerals that have resistivities 10 times lower than those of the surrounding rocks (Nelson and Anderson, 1992). Fine-grained sediments, such as clay-rich alluvium, marine shales, and other mudstones, are normally conductive from a few ohm-m to a few tens of ohm-m (Keller, 1987; Palacky, 1987). Metamorphic rocks (nongraphitic) and unaltered, unfractured igneous rocks are normally moderately to highly resistive (a few hundreds to thousands of ohm-m). Carbonate rocks can have similarly high resistivities depending on their fluid content, porosity, and impurities (Keller, 1987; Palacky, 1987). Fault zones may be moderately conductive (tens of ohm-m) when composed of rocks fractured enough to have hosted fluid transport and consequent mineralogical alteration (Eberhart-Phillips and others, 1995). Higher subsurface temperatures cause higher ionic mobility that reduces rock resistivities (Keller, 1987; Palacky, 1987). Tables of electrical resistivity for a variety of rocks, minerals, and geological environments are in Keller (1987) and Palacky (1987).

Obtaining a reliable AEM-derived resistivity model requires complete system characterization including 1) geometry; 2) frequencies and bandwidth; 3) transmitter waveform characteristics; 4) timing; 5) and 6) accurate modeling (Christiansen and others, 2011). Poor AEM modeling assumptions can lead to errors in the resulting resistivity models and, in turn, the hydrologic and geologic interpretations (Viezzoli and others, 2013). These effects can include erroneous resistive or conductive layers and skewed estimates of depth to interfaces. Inverting AEM data with an incomplete system description will commonly lead to a realistic, but incorrect earth resistivity model that fits the data to within measured or estimated data errors. This is why it is imperative that the AEM system be completely characterized and understood.

AEM Measurements

The AEM measurements were completed with the SkyTEM 304 system. This system was selected for its ability to detect the geology commonly found in eastern Nebraska (Abraham and others, 2011a). The selected AEM system is a rigid frame, dual-moment

Transient Electromagnetic (TEM) system developed over the past ten years (Sørensen and Auken, 2004). In contrast to the other TEM systems, this system has the receiver coil positioned slightly behind the transmitter wire in a ñnullò position, where the intensity of the primary field is minimized. The AEM system was initially designed for groundwater mapping, and to this end employs two transmitter moments with different currents and different numbers of transmitter wire turns. The low current, or low moment (LM) mode, with a moment of 3,140 (number of turns × current × amp × area (m^2) (NIA)), is used to record early-time gates which constrain near-surface information, while the high current, or high moment (HM) mode, with a moment of 145,000 NIA, improves the signal-to-noise ratio at late time gates.

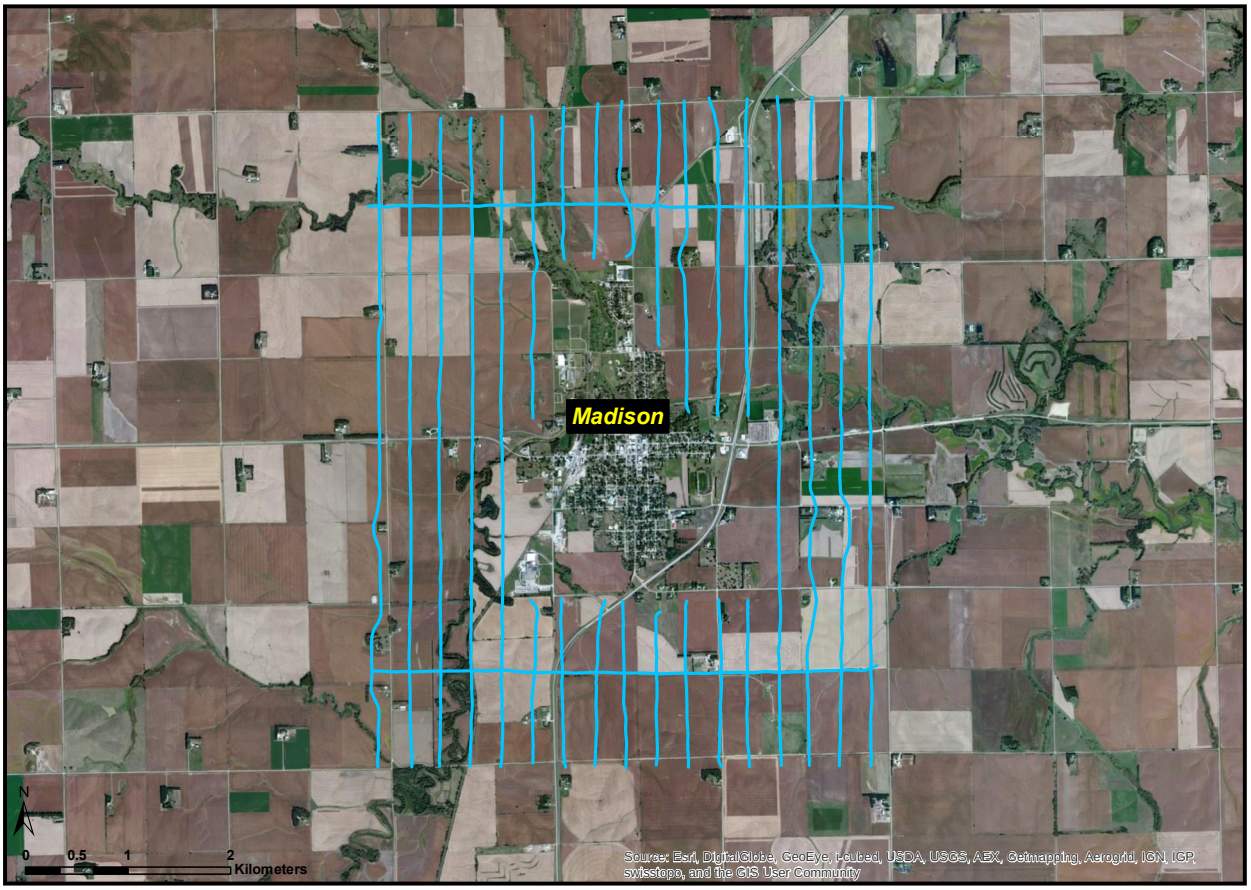


Figure 2 – Flight line locations over the Project Area.

The AEM system used in this study has a transmitter area of 314 m^2. The AEM system records time gates from 1.6 ε s to 11 ms. The gates interpreted in the Madison survey fall between 9.6 ε s and 7.0 ms, with the latest recorded gates being too noisy to be used, and the gates before 5 ε s contaminated by residual primary field.

The AEM system was calibrated to a ground test site in Lyngby, Denmark using the process described in HGG (2010); HGG (2011); and Foged and others (2013). Approximately 100-line km were flown within the Madison, Nebraska area (Figure 2). Flight operations were conducted on August 12, 2013.

AEM Data Processing

The Aarhus Geophysics Workbench version 4.1.1.765 (Aarhus Geophysics, 2013) was used for the processing and inversion of the AEM data. The Aarhus Geophysics Workbench was developed by the Hydrogeophysics Group at the University of Aarhus in Aarhus, Denmark (Auken and Christiansen, 2004; Viezzoli and others, 2008; Auken and others, 2009; Christiansen and Auken, 2012; Aarhus Geophysics, 2013). This program is specifically well suited for editing AEM data and removing couplings to power lines and pipelines.

Automatic Processing

The AEM data were first run through automatic processing algorithms within the processing program. The GPS locations were filtered using a stepwise second order polynomial filter of 9 seconds, with a step length of 0.5 seconds. Filters were also applied to both of the tilt meter readings, including a median filter of 3 seconds and an average filter of 2 seconds. The AEM data are corrected for tilt deviations from level. The altitude data are corrected using a series of two polynomial filters. The length of both eighth-order polynomial filters were set to 30 seconds with shifts length of 6 seconds. The lower and upper thresholds were 1 and 30 meters, respectively.

The AEM data are run through several different filters including slope, sign, and trapezoidal filters. The cap sign filters cull data when the value changes sign and began at $1.5e^{-5}$ seconds for the low moment and $1e^{-4}$ seconds for the high moment. The noise level for the cap sign filter was set to $5e^{-7}$ $ms*v/m^2$ with a slope of -0.5 for the low moment and $2e^{-7}$ $ms*v/m^2$ with a slope of -0.5 for the high moment. The cap slope filter removed four time gates before the change in sign for both moments. The cap slope filters use the same time period, noise level, and noise slope as the cap sign filter and culls sounding data if the second order derivative of the dB/dt curve is outside of the minimum and maximum slope. The minimum slope was -0.5 and the maximum was 0.5 for both moments. The average sign filter works on the averaged data, removing data when a change in sign occurs. The average slope filters were not used on this data set. The trapezoidal filters are used to average the AEM sounding data. The times used to define the trapezoidal filters for the low moment are $1e^{-5}$, $1e^{-4}$, and $1e^{-3}$ with widths of 2, 5 and 10 seconds. The times used to define the trapezoid for the high moment are $1e^{-4}$, $1e^{-3}$ and $1e^{-2}$ with widths of 5, 10, and 20 seconds. The spike factor and minimum number of gates were both set to 25 percent for both soundings.

Manual Processing and Laterally Constrained Inversions

After the implementation of the automatic filtering, the AEM data were examined manually by using a sliding 2-minute time window. The data were examined for possible coupling with surface and buried metal as well as for late time gate noise levels. Data impacted by these were removed. In addition, the results of the automatic filtering processes were monitored. In some instances, AEM data that were removed by the automatic filters were re-included.

The AEM data were then inverted using a laterally constrained inversion (LCI) algorithm (Auken and Christiansen, 2004). A starting model consisting of 19 layers with starting resistivities of 40 ohm-m were used. This model went to a depth of 300 meters with the thickness of the layers increasing with depth. The vertical resistivity standard deviation was set to 2, while the lateral resistivity standard deviation was set to 1.3 for the first 11 layers, 1.25 for layers 12 through 15, and 1.2 for layers 16 through 19. Following the LCI, profile and depth slices were created to examine the results of the inversion. When remaining couplings were located, the data were again manually removed and additional LCIs were performed.

Spatially Constrained Inversion

If the results of the second LCI were determined to be free of couplings, a spatially constrained inversion (SCI) (Viezzoli and others, 2008) was performed on the data. After processing and de-coupling 98 line km of data were included in the SCI. The starting model and standard deviations used were the same as those described for the LCI 40 ohm-m. Additionally the SCI creates sections in which the inversions are spatially constrained. The approximate section size selected was 100 soundings, with a minimum of 50.

The inversion results were once again examined using profiles and depth slices. If any remaining Coupling were detected they were removed and the inversions run again. Depth of Investigation (DOI) was calculated using the method described by Christiansen and Auken (2012) on the Madison dataset. Maximum DOI was 252 meters, minimum DOI was 25 m, and average DOI was 178 meters. The resulting models are then exported in ASCII file formats to be displayed and interpreted.

Data Display and Interpretation

The interpretation of the AEM inversion resistivity model was completed in a Geographical Information System (GIS) that provided X, Y, and Z coordinates (PitneyBowes, 2013). Prior to interpreting the AEM data, several complementary datasets were included and graphically displayed in 2-D and 3-D GIS environments. Complementary data included test-hole lithology, test-hole geophysical logs (including natural gamma and electrical resistivity), TDEM resistivity models, airborne measurements of the intensity of 60-hertz power-line interference, airborne measurements of the magnetic total-field intensity, airborne photographs, and the 90-m digital elevation model (DEM). Other maps, identifying roads, power lines, pipelines, towns, and geology, were used. The AEM inversions were displayed as colored resistivity sections within the GIS environment. The resistivity data were plotted using the same color scale, and all of the datasets were placed in the same projected coordinate system. This allowed the data to be examined at many scales and for data to be interactively displayed and/or hidden in order to fully examine how the geophysical data interrelate with complementary datasets.

3-D voxel models of the resistivity were created with a 50 meter square cell and a thickness related to the 19 layer inversion model layer (see Appendix 1). These voxel models were then thresholded and interpreted in the same 3-D GIS environment as the AEM sections. Cross-sections, slices and volumes were calculated and used in interpretation of the Madison data and compared directly to borehole lithologic data.

Due to Federal Aviation Administration regulations, no AEM data were acquired over the built up areas of Madison, Nebraska (Figure 2). Thus, the subsequent interpretation of the bedrock topography and the volume of aquifer materials have a gap in the area were no AEM data were acquired. Subsequent images of the data have a gap in the area of no data collection.

Hydrogeology of the Project Area

Geologic Setting

The Madison survey area is situated within Nebraskaôs Rolling Hills Topographic Region (UNL-Conservation and Survey Division, 1973). This physiographic setting is predominately a hilly landscape with moderate to steep slopes and rounded hilltops (uplands) separated by local drainages. The hills in the area are composed of glacial till mantled by wind-transported silt deposits (loess). Relative relief within the project area is approximately 140 feet, with the highest elevations in the upland hills south of the city and the lowest elevation along Union Creek on the northeast edge of Madison. Union Creek meanders southwest to northeast in the project area and is fed by intermittent Taylor Creek on the west side of Main Street on the north side of Madison. No current flow data is available for Union Creek at Madison. However, the U.S. Geological Survey has historical Union Creek flow data from 1978 to 1993 available. Average daily flow in Union Creek over this period is 1.3 cubic meters per second (45.4 cubic feet per second). The perennial flow in this drainage indicates that stream flow is likely supported throughout the year by a groundwater component.

The geology of southeast Madison County is characterized by unconsolidated Quaternary-age deposits overlying Tertiary and Cretaceous-age bedrock. The City of Madison is situated near the western edge of eastern Nebraskaôs glaciated terrain. During the Pleistocene Epoch (2.5 million years to 10,000 years before the present) of the Quaternary Period, the Laurentide Ice Sheet advanced and retreated across northeast Nebraska (Dyke and others, 2002; Mathews, 1974). The several-hundred meter thick ice sheet scoured the pre-glaciated terrain and deposited till (unsorted geologic material ranging in size from clay to boulders) and outwash deposits (predominately sand and gravel). Where ice sheet movement stagnated, areas of accumulated till would result in modern-day landform features known as moraines. The University of Nebraskaôs Conservation and Survey Division (CSD) Till Thickness Map indicates that the glacial till in the Madison area is less than 45 meters thick, and in most areas, till thickness is less than 15 meters. Outwash deposits resulted from melt water from the glacier transporting, sorting, and depositing coarse materials within close proximity as well as at distal reaches from the ice margin. These deposits form modern-day aquifers across much of eastern Nebraska and will be discussed further in the following sections.

Mantling the till throughout much of eastern Nebraska is wind-deposited silt called loess. This silt can exceed 30 meters in thickness in southern Madison County (Mason and others, 2006).

Hydrogeology of Quaternary Deposits

Aquifers exist where thick, aerially extensive outwash sediments were deposited at and beyond the ice sheet margins. In eastern Nebraska, depths to these aquifers vary depending on location- some outwash-derived aquifers can be less than 2 meters below the land surface while others can be buried by tens of meters of till. In Madison and surrounding counties, several modern day drainages are underlain by these outwash sediments, including West and East Maple Creeks in Colfax County. The presence of the ice sheet during the pre-Illinoian time altered the routes of previously eastward draining streams. Many of these streams followed drainages created by melt water draining west/southwest from the ice margin (Reed and Dreezen, 1965). In other areas, outwash deposits are completely buried by till and loess, and no modern-day surface expression or drainage reveals their presence.

In the area surrounding Madison, outwash deposits with varying thicknesses are present throughout much of the subsurface and form the present-day aquifers. Most of these sediments are overlain by clay and/or silt ranging from less than 5 to over 20 meters in thickness. Productivity of wells tapping these unconsolidated sediments depends on the thickness, extent and percentage of fine materials (clay, silt, very fine sand) present as well as the quality of well construction. Review of well records from the Nebraska Department of Natural Resources (NDNR) Registered Well Database can provide insight into aquifer productivity across the project area. Figure 3 shows the distribution and use of registered wells in the legal sections surrounding Madison. Irrigation wells account for a majority of the wells in the area, with 69 total present within the map in Figure 3. Of these, 64 have pumping rates in the records with an overall average pumping of 3.3 cubic meters per minute (m^3/min) (863 gallons/minute (gpm)) and an average completion depth of 59.7 meters below the ground surface (bgs). Domestic wells are present in the Madison area, primarily to the south and east of the city. The average pumping rate for these wells is 0.08 m^3/min (21 gpm) and the average domestic well depth is 58 meters bgs. NDNR records also indicate four registered industrial wells located in Madison. These wells average 4.1 m^3/min (1,075 gpm) from an average depth of 42 meters bgs. The capacity of these wells indicates that productive aquifer materials exist in the subsurface beneath the city limits. It should be noted that these pumping rates have not been independently verified, and are likely to differ from when the well was originally constructed and registered.



Figure 3 – Locations of registered wells by use and CSD test holes in the Project Area.

Cretaceous Geology and Aquifer Potential

Bedrock information from the CSD indicates that the Quaternary deposits in the Madison area are underlain by Cretaceous-age shale of the regionally-extensive Niobrara Formation as well as a narrow band of the Tertiary-age Ogallala Group beneath the northern two-thirds of the Project Area. However, evaluation of test hole logs from the NDNR Registered Well Database by XRI did not reveal the presence of sediments indicative of the Ogallala Group beneath Madison. The three CSD test holes (Figure 3) only reach a maximum depth of 24 meters and do not penetrate the full thickness of the Quaternary deposits. These test holes would likely provide the basis for the regional bedrock mapping, therefore it is unclear why Ogallala Group material is mapped beneath Madison, especially considering that the continuously mapped portion of the regionally extensive Ogallala Group is about 19 kilometers west of Madison.

The Niobrara Formation is not a productive aquifer unit, as its primary lithologies are clayey chalk, limestone, and shale. The maximum reported thickness of the Niobrara Formation is 570 feet; however, the thickness of this formation is not known beneath Madison (Burchett, 1986). It is likely that the Niobrara Formation is much thinner as Madison sits atop its eastern margin. Several other bedrock units, including sandstone of the Dakota Group underlies the Niobrara Formation. The Dakota Group is utilized as an aquifer across much of eastern Nebraska at depths ranging from 150 to over 300 meters.

The capability of the AEM instruments to penetrate to these depths in the subsurface reveals the presence of potential bedrock aquifer material beneath conductive bedrock material in the southeast quarter of the Project Area.

Interpretation of AEM Results

Map of the Principal Aquifer

The AEM resistivity model reveals the character of the Quaternary deposits across the project area with a level of three-dimensional detail that would be unobtainable with the current inventory of borehole information. Interpretive imagery from the AEM survey are presented in Appendix 1, and each figure in the appendix will be denoted with the letter A. Figure A-1 displays the land surface coverage that corresponds to the subsurface areas displayed in Appendix 1. Output generated from the survey (Figures A-2 and A-3) shows distinct contrasts between electrically conductive materials (clay and silt) and more electrically resistive sediments (coarse deposits). The conductive zones are interpreted as glacial till and loess, whereas the resistive areas indicate the extent and thickness of the principal aquifer (hereafter referred to as ñaquiferò) in the project area. There is no evidence in the historical work that saline water is present in the survey area, which would cause the electrical conductivity to increase. The geologic descriptions from borehole logs across the area match the geophysical results well, although deviations occur in some areas as most boreholes are not located directly along a survey flight-line. In addition to the Quaternary deposits, the character of the bedrock surface has been isolated to display the subsurface topography beneath the Quaternary system (Figures A-4 through and A-8). The subsurface topography is directly related to the advance and subsequent erosion created by the ice sheet.

The principal aquifer is delineated by a resistivity threshold of 23 ohm-m as displayed in Figures A-5 through A-9. Higher resistivity values correspond to areas in the subsurface with greater potential for productive aquifer materials. The 23 ohm-m level and above represent areas where there is greatest confidence in the location of the principal aquifer. The most extensive area with the highest resistivities detected in the survey is located in the southeast quarter of the project area beneath the upland hills south and southeast of Madison. Figures A-14, A-15, and A-17 show this area in pink. The deposits in this area approach 40 ohm-m in resistivity and are interpreted as glacial outwash. In this area, the resistive zones exceed 50 meters in thickness and extend from the Union Creek valley to the eastern and southern edges of the Project Area. Depth to the top of these materials ranges from 10-20 meters. A review of the limited number of irrigation wells from the NDNR Registered Well Database would indicate this portion of the aquifer supports wells that are registered to pump 700 to 850 gallons per minute (gpm).

The second high-resistivity area is found on the north edge of Madison in the area underlying the present-day valley of the Taylor Creek watershed. Figure A-16 shows this resistive area near registered well no. G-152749. The coarse deposits approach 75 meters in thickness in the portion of the Project Area, but are much more limited in extent in comparison to the area southeast of Madison (Figure A-8). Registered pumping rates for irrigation wells that tap these coarse deposits range from 700 to 1,000 gpm. These deposits extend eastward and slightly southward to the east project area boundary with a relatively

uniform thickness but with slightly lower resistivities. This entire northern zone of resistive materials are overlain by 10 to 50 meters of conductive (fine) deposits that thicken eastward. Similar to the southeast resistive zone, very few irrigation wells are present in the northeast portion of the project area along the north tie-line displayed in Figure A-16 and the north-south flight line in Figure A-15.

One additional isolated zone of resistive material is present in the southwest corner of the Project Area. This area ranges from 15-25 meters in thickness and is overlain by 10-20 meters of conductive material (Figures A-8 and A-17).

In summary, the aquifer in the project area is most extensive south and southeast of Madison where highly resistive materials are present beneath the upland hills. Most of the area from the Union Creek valley to the eastern boundary south of Madison is underlain by these resistive materials and are mantled by 10-20 meters of conductive deposits. North of Madison, a resistive zone is present beneath the Taylor Creek drainage and extends eastward and somewhat southward to the eastern project area boundary. The highest resistivities are found in an isolated area immediately beneath the present-day valley. Resistivities dissipate somewhat and overall depth to the top of the coarse deposits increases eastward, but the overall aquifer remains uniform in thickness through the northeast portion of the project area.

Estimate of Aquifer Volume

Three-dimensional digital representation of the subsurface resulting from the AEM method provides users the ability to more accurately estimate total aquifer volume and the amount of extractable water. For this calculation, the 23 ohm-m threshold is used to separate aquifer from non-aquifer materials with any value below this level to be considered non-aquifer material. As described previously in this report, the higher a materialôs resistivity the more likely it is to be an aquifer. Two estimates for specific yield were chosen for the 23 ohm-m and greater aquifer volume. In absence of any historical data on specific yield in the Madison area, the low values for medium sand (0.10) and fine gravel (0.21) (Fetter, 1994) were chosen to capture the range of possible water volume stored within the aquifer in the Project Area. These two values are considered to be end members of the most likely range of specific yield in the Project Area, and hence, most closely estimate the volume of water within the aquifer in the AEM flight area. The total volume of extractable water calculated by using specific yield values of 0.1 and 0.21 range from 49.5 to 103.9 million cubic meters, with an average value of 76.7 million cubic meters of extractable water in storage (Table 1).

Table 1. ï Estimates of extractable water content in the principal aquifer underlying the AEM flight area.

Resistivity Threshold (ohm-m)	Aquifer Volume (m^3)	Specific Yield	Extractable Water Volume (millions m^3)
23	4.95×10^8	0.10	49.5
23	4.95×10^8	0.21	103.9
		Average	76.7

Relationship to Current Test Holes and Production Groundwater Wells

Only three CSD test holes are present within the Madison area, and unfortunately these holes are situated within the area of Madison that did not fall directly beneath the AEM flight lines. Therefore, direct comparison with CSD-quality test holes was not possible for this project. Fortunately, several borehole logs from the NDNR Registered Well Database were available to review for comparison with the AEM output. XRI assessed the lithology of each of these logs and assigned Unified Soil Classification System soil descriptor codes to each unique lithologic interval. It should be noted, however, that the quality of the borehole logs from the registered wells varies greatly from log to log and were not subject to the same quality assurance and quality control as the CSD logs. The log data from all of the reviewed well locations were compiled and included in the AEM processing software for overlay comparison with the geophysical results.

Figure 4 shows close-in comparisons of the lithologic descriptions and the AEM results from the cross-sections shown in Appendix 1. Included is a comparison of registered well no. G-152749 that is located near the north west-east flight line that captures the high-resistivity zone on the north side of Madison, and registered well no. G-81794 situated near the south west-east flight line that crosses the southern high-resistivity zone. The comparison of the boreholes and the geophysical results match closely. It should be noted that very few well or test hole locations are directly on a flight line, and that slight deviation should be expected between the borehole lithology and the geophysical information due to the inherent complexity of glacial depositional environments.

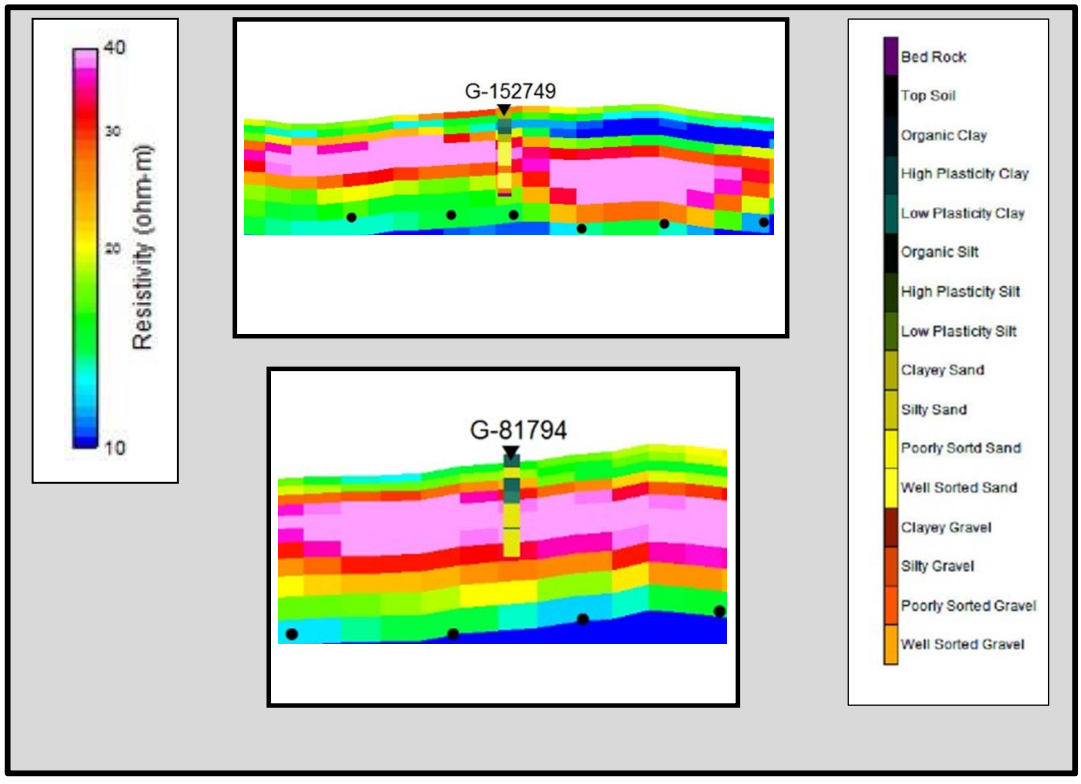


Figure 4 – Comparison of the subsurface resistivity (scale on the left) and the lithologic classifications at two borehole log locations.

As mentioned in prior sections, it is apparent that some of the most resistive zones mapped in the AEM survey in the Madison area contain a relatively small number of extraction wells. It is unclear as to what the primary factors are influencing this limited distribution of wells. It is possible that land ownership, terrain, or soil type could play a role in the present-day distribution of extraction wells.

Estimated Potential Recharge Areas

Recharge to the groundwater flow system depends on multiple factors, including precipitation rate, soil type, composition and thickness of the vadose zone, surface slope, density and type of vegetation, and land use practice. The greatest chance for recharge in the survey area occurs in areas where the landscape is relatively flat and where the upper soil horizon and vadose zone allow for rapid infiltration and downward transmittal of water below the root zone.

Potential for recharge to the groundwater flow system in the Madison survey area occurs in areas where surface topography is generally flat and relatively permeable soil is present. The landscape is generally flat in the northern half of the city and to the north/northeast in the lowland valley of Union Creek. The soils in this area are typically silt and silt-clay loams with very low slopes (0 to 1 percent) and moderately high capacities to transmit water (Hammond and others, 1984). To the west and south of the city, the upland terrainôs hummocky character and greater presence of till and loess limits recharge to the underlying aquifer materials, with the exception of areas where surface impoundments capture surface runoff and provide focused recharge into the subsurface.

Szilagyi and Jozsa (2005) estimated a net recharge to groundwater ranging from 49 to 60 millimeters in the Madison area based on calculations from a statewide water balance modeling study. This range in precipitation equates to about 7 to 9 percent of total annual precipitation in the area (685 millimeters/year) (www.usclimatedata.com).

Summary and Recommendations

The need for future water management decisions for the city of Madison has increased the need for detailed hydrogeologic frameworks for the area around the city. Demand for increased groundwater development near the city for various uses has motivated the city to evaluate whether the current supply can be expanded without degradation to the existing wells. Recent drought conditions (2012) in the area have increased interest from other government entities to look for additional groundwater supply. If new groundwater development is expanded into the area of the city wells, the city needs to understand the aquifer geometry, characteristics, connection with surface water, adjacent aquifers and water production wells. The three (3) Conservation and Survey Division (CSD) test holes in or near the area are vital to the understanding of groundwater, but they cannot provide enough information to complete a detailed hydrogeologic framework.

Therefore an airborne electromagnetic (AEM) survey was performed to supplement the test hole information and in turn used to develop a new hydrogeologic framework. The results of the study show that the principal aquifer exists in zones within the project area. These

deposits are not continuous across the project area. There are two main zones of aquifer material and they lie southeast and north of the city. The aquifer material is mostly sand and gravel deposits left by the glacial activity of the past. The amount of recoverable water within the mapped area is estimated to be 76,700,000 cubic meters.

The small area mapped by this project provides detailed information on the aquifers near the city. The results show the orientation and geometry of the aquifers within the flight area. They also show that those aquifers extend beyond the study boundary to the north, east and southeast. Thus, the total amount of water in storage available to the current wells is unknown. We recommend that additional AEM surveys with framework development be extended to the north, east and southeast to determine aquifer boundaries and volume. We also recommend that an aquifer test be completed to understand the actual characteristics of the system and provide new estimates of groundwater in storage.

Bibliography

Abraham, J.D., Bedrosian, Asch, T.H., Ball, L.B., Cannia, J.C, Philips, J.D., and Lackey, S. 2011a. Evaluation of Geophysical Techniques for the Detection of Paleochannels in the Oakland Area of Eastern Nebraska as Part of the Eastern Nebraska Water Resource Assessment: U.S. Geological Survey Scientific Investigations Report 2011-5228, p. 40. http://pubs.usgs.gov/sir/2011/5228/

Abraham, J.D., Cannia, J.C, Bedrosian, P.A., Johnson, M.R., Ball, L.B., and Sibray, S.S. 2011b. Airborne Electromagnetic Mapping of the Base of the Aquifer in Areas of Western Nebraska: U.S. Geological Survey Scientific Investigations Report 2011-5219. http://pubs.usgs.gov/sir/2011/5219/

Auken E., and Christiansen, A.V. 2004. Layered and laterally constrained 2D inversion of resistivity data, Geophysics, 69, 752-761, doi: 10.1190/1.1759461.

Auken, E., Christiansen, A.V., Westergaard, J.H., Kirkegaard, C., Foged, N., Viezzoli, A. 2009. An integrated processing scheme for high-resolution airborne electromagnetic surveys, the SkyTEM system, Exploration Geophysics, 2009, 40, 184ï 192, doi:10.1071/EG08128.

Aarhus Geophysics. 2013. Aarhus Workbench, version 4.1.1.765, http://www.aarhusgeo.com/content/software/workbench/aarhus-workbench.html

Burchett, R. R., 1986, Geologic Bedrock Map of Nebraska: Nebraska Geological Survey. Scale 1:1 million.

Christiansen A.V., and Auken, E. 2012. A global measure for depth of investigation, Geophysics, 77, 171-177, doi:10.1190/geo2011-0393.1.

Christiansen, A.V., Auken, E., and Viezzoli, A. 2011. Quantification of modeling errors in airborne TEM caused by inaccurate system description, Geophysics, 76, 43-52, doi:10.1190/1.3511354.

Dyke, A.S., Andrews, J.T., Clark, P.U., England, J.H., Miller, G.H., Shaw, J., and J.J. Veillette. 2002. The Laurentide and Innuitian Ice Sheets during the Last Glacial Maximum. Quaternary Science Reviews. Vol. 21, No 9-31.

Eberhart-Phillips, D., Stanley, W.D., Rodriguez, B.D., and Lutter, W.J. 1995. Surface seismic and electrical methods to detect fluids related to faulting: Journal of Geophysical Research, v. 100, no. B7, p. 12919ï 12936.

Fetter, C.W. 1994. Applied Hydrogeology, Third Edition. MacMillan College Publishing Company, New York.

Fitterman, D. V., and M. Deszcz-Pan. 1998. Helicopter EM mapping of saltwater intrusion in Everglades National Park, Florida: Exploration Geophysics, 29, 240ï 243, doi: http://dx.doi.org/10.1071/EG998240.

Foged, N., Auken, E., Christiansen, A. V. and Sørensen, K. I. 2013. Test site calibration and validation of airborne and ground based TEM systems. Geophysics, 78, 95ï 106. doi: 10.1190/geo2012-0244.1.

Hammond, C.L., Vanek, W., Rieke, D., Willoughby, M.E., Kuzila, M., Nass, A.T. and R. Staples. 1984. Soil Survey of Madison County, Nebraska. U.S. Department of Agriculture - Natural Resource Conservation Service and the University of Nebraska Conservation and Survey Division.

HydroGeophysics Group, Aarhus University, Denmark, GUIDELINE AND STANDARDS FOR SKYTEM MEASUREMENTS, PROCESSING AND INVERSION, November 2011, version 2.5., http://www.hgg.geo.au.dk/rapporter/SkyTEMGuideEN.pdf

HydroGeophysics Group, Aarhus University, Denmark, GUIDELINE AND STANDARDS FOR SKYTEM MEASUREMENTS, PROCESSING AND INVERSION, November 2011, version 2.5., http://www.hgg.geo.au.dk/rapporter/SkyTEMGuideEN.pdf

HydroGeophysics Group. 2010. Aarhus University, Denmark, Validation of the SkyTEM system at the extended TEM test site, 2010, http://www.hgg.geo.au.dk/rapporter/Validating_SkyTEM_Test_Site_2010.pdf

Jørgensen, F, Scheer, W, Thomsen, S, Sonnenborg, T.O., Hinsby, K., Wiederhold, H., Schamper, C., Burschil, T., Roth, B., Kirsch, R., and Auken. E. 2012. Transboundary geophysical mapping of geological elements and salinity distribution critical for the assessment of future sea water intrusion in response to sea level rise: Hydrol. Earth Syst. Sci., 16, 1845ï 1862, doi: http://dx.doi.org/10.5194/hess-16-1845-2012

Jørgensen, F., Sandersen,P.B.E., Auken, E. 2003. Imaging buried Quaternary valleys using the transient electromagnetic method, Journal of Applied Geophysics, 53, 199- 213, doi:10.1016/j.jappgeo.2003.08.016.

Keller, G.V. 1987. Rock and mineral properties, in Nabighian, M.N., ed., Electromagnetic methods in applied geophysics theory: Tulsa, Oklahoma, Society of Exploration Geophysicists, v. 1, p. 13-51.

Keller, G.V. 1989. Electrical properties, in Carmichael, R.S., ed., Practical handbook of physical properties of rocks and minerals: Boca Raton, Florida, CRC Press, 359-427.

Lawrie, K.C., Brodie, R.S., Tan, K.P., Gibson, D., Magee, J., Clarke, J.D.A., Halas, L., Gow, L., Somerville, P., Apps, H.E., Christensen, N.B., Brodie, R.C., Abraham, J., Smith, M., Page, D., Dillon, P., Vanderzalm, J., Miotlinski, K., Hostetler, S., Davis, A., Ley-Cooper, A.Y., Schoning, G., Barry, K. and Levett, K. 2012. BHMAR Project: Data Acquisition, processing, analysis and interpretation methods. Geoscience Australia Record 2012/11. 826p.

Mason, J. A., Bettis, A. E., Roberts, H. M., Muhs, D. R., and Joeckel, R. M., 2006, Last glacial loess sedimentary system of eastern Nebraska and western Iowa; AMQUA post-meeting field trip no. 1; *in*, Guidebook of the 18th Biennial Meeting of the American Quaternary Association, R. Mandel, ed.: Kansas Geological Survey, Technical Series 21, p. 1-1ï 1-22.

Mathews, W.H. 1974. Surface Profiles of the Laurentide Ice Sheet in its Marginal Areas. Journal of Glaciology. Vol. 13, No. 7.

Møller, I., Søndergaard, V.H., Jørgensen, F., Auken, E., and Christiansen, A.V. 2009. Integrated management and utilization of hydrogeophysical data on a national scale, Near Surf. Geophysics, 7, 647-659, doi:10.3997/1873-0604.2009031.

Muhs, D.R., Bettis III, E.A., Aleinikoff, J.N., McGeehin, J.P., Beann, J., Skipp, G., Marshall, B.D., Roberts, H.M., Johnson, W.C. and R. Benton. 2008. Origin and paleoclimate significance of late Quaternary loess in Nebraska, Evidence from stratigraphy, chronology, sedimentology, and geochemistry. Geological Society of America Bulletin, November/December 2008.

Nebraska Department of Natural Resources Registered Well Database. Accessed in December 2013 at http://dnrdata.dnr.ne.gov/wellscs/Menu.aspx.

Nelson, P.H., and Anderson, L.A. 1992. Physical properties of ash flow tuff from Yucca Mountain, Nevada: Journal of Geophysical Research, v. 97, no. B5, p. 823ï 6841.

Oldenborger, G.A., Pugin, A.J.-M., and Pullan, S.E. 2013. Airborne time-domain electromagnetics, electrical resistivity and seismic reflection for regional three-dimensional mapping and characterization of the Spiritwood Valley Aquifer, Manitoba, Canada, Near Surf. Geophysics, 11, 63-74, doi:10.3997/1873-0604.2012023.

Paine, J.G., and Minty, B.R.S. 2005. Airborne hydrogeophysics, Hydrogeophyiscs, 50, 333-357, doi:10.1007/1-4020-3102-5_11.

Palacky, G.J. 1987. Resistivity characteristics of geologic targets, in Nabighian, M.N., ed., Electromagnetic methods in applied geophysics theory: Tulsa, Oklahoma, Society of Exploration Geophysicists, v. 1, 53-129.

PitneyBowes. 2013. Encom Profile PA Analyst Software, Version 12.0.0, http://www.encom.com.au/template2.asp?pageid=16

Reed, E.C. and V.H. Dreezen. 1965. Revision of the classification of the Pleistocene deposits of Nebraska. Nebraska Geological Survey Bulletin No. 23. 65 p.

Sørensen, K., and Auken, E. 2004. SkyTEM - A new high-resolution helicopter transient electromagnetic system, Exploration Geophysics, 35, 191ï 199, doi: 10.1071/EG04194.

Szilagyi, J., Harvey, F.E., and J.F. Ayers. 2005. Regional Estimation of Total Recharge to Ground Water in Nebraska. Groundwater. Vol. 43, No. 1, p. 63-69

University of Nebraska-Lincoln Conservation Survey Division. 1973. State of Nebraska Topographic Regions Map. Accessed online at: http://digitalcommons.unl.edu/cgi/viewcontent.cgi?article=1062&context=caripubs on December 3, 2013.

University of Nebraska-Lincoln Conservation Survey Division. 1998. The Groundwater Atlas of Nebraska. Resource Atlas No. 4a/1998.

University of Nebraska-Lincoln Conservation Survey Division Online Statewide Test Hole Database. Accessed multiple events in December 2013. Accessible at: http://snr.unl.edu/data/geologysoils/NebraskaTestHole/NebraskaTestHoleIntro.asp.

University of Nebraska-Lincoln Conservation Survey Division. State of Nebraska Glacial Till Deposit Map. Accessed online at: http://snr.unl.edu/data/geographygis/NebrGISgeology.asp#till

Viezzoli, A, Jørgensen, F., and Sørensen, C. 2013. Flawed Processing of Airborne EM Data Affecting Hydrogeological Interpretation: Groundwater, 51, No. 2, 191ï 202, doi: http://dx.doi.org/10.1111/j.1745-6584.2012.00958.x

Viezzoli, A., Christiansen, A.V., Auken, E., and Sørensen, K. 2008. Quasi-3D modeling of airborne TEM data by spatially constrained inversion, Geophysics, 73, 105-113, doi:10.1190/1.2895521.

Viezzoli, A., Tosi, L., Teatini, P. and Silvestri, S. 2010. Surface waterï groundwater exchange in transitional coastal environments by airborne electromagnetics: The Venice Lagoon example, Geophysical Research Letters, 37, L01402, doi:10.1029/2009GL041572.

Wynn, J. 2002. Evaluating groundwater in arid lands using airborne magnetic/EM methods, an example in the southwestern U.S. and northern Mexico, The Leading Edge, 21, 62-64, doi:10.1190/1.1445851.

Appendix 1- AEM Interpretive Imagery

List of Figures in Appendix 1

Figure A-1: Aerial imagery of land surface area that corresponds to the subsurface plots covered by the AEM flight lines surrounding Madison that are displayed in the Appendix I figures.

Figure A-2: 3-D image displaying electromagnetic response of the subsurface along each flight line surrounding Madison.

Figure A-3: Image displaying the 3-D resistivity model the AEM survey.

Figure A-4: 3-D image displaying 3D resistivity model of the AEM survey contact between the Quaternary units and underlying bedrock demarcated as a horizontal layer.

Figure A-5: 3-D image of subsurface areas exhibiting resistivity values of 23 ohm-m or greater with the Quaternary unit-bedrock contact and depth of bedrock penetrated displayed.

Figure A-6: 3-D image of all Quaternary deposits and bedrock units with resistivity values of 23 ohm-m or greater.

Figure A-7: 3-D image of Quaternary deposits only with resistivity levels at 23 ohm-m or greater above the bedrock surface.

Figure A-8: Distribution of the principal aquifer (23 ohm-m or greater) overlying the bedrock surface.

Figure A-9: Distribution of the principal aquifer (as displayed in Figure A-8) with the AEM flight lines and land surface for reference of the aquifer location in relation to the city area.

Figure A-10: Location and distribution of bedrock units with resistivity levels of 23 ohm-m or greater underling the project area.

Figure A-11: Location and distribution of bedrock units with resistivity levels at 23 ohm-m or greater underlying the bedrock surface. Also displayed are the borehole log locations with color-coded lithologies.

Figure A-12: South to north cross section along an AEM flight line near the western edge of Madison.

Figure A-13: South to north cross section along an AEM flight line northeast of Madison.

Figure A-14: South to north cross section along an AEM flight line southeast of Madison exhibiting an extensive resistive zone.

Figure A-15: South to north cross section along an AEM flight line east of Madison exhibiting resistors in the Quaternary units and in the bedrock on the southern quarter of the flight line.

Figure A-16: West to east cross section along the northern tie-line near the northern edge of Madison.

Figure A-17: West to east cross section along the southern tie-line south of Madison.

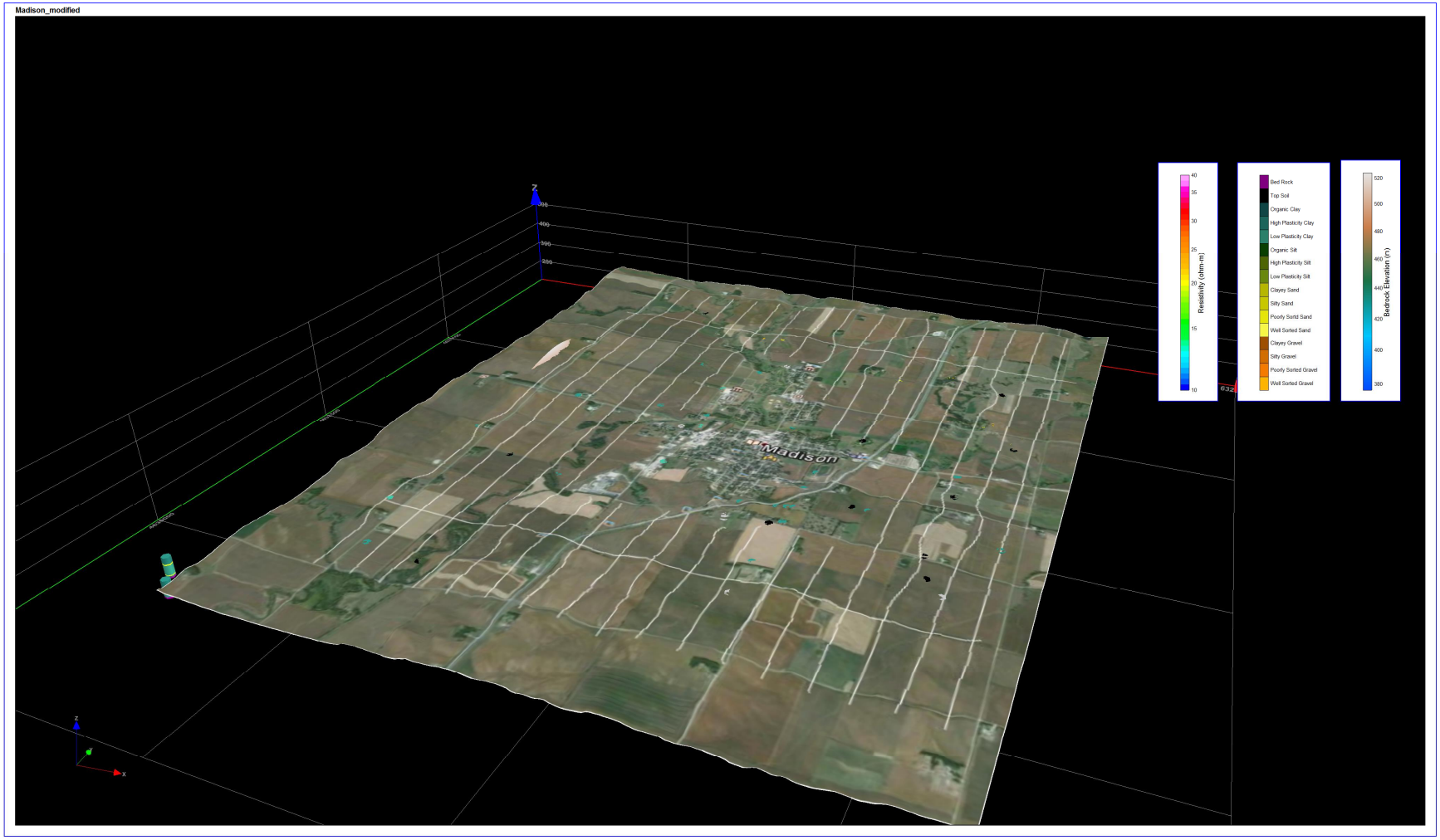


Figure A-1 – Aerial imagery of land surface area that corresponds to the subsurface plots covered by the AEM flight lines (gray lines) surrounding Madison that are displayed in the Appendix I figures.

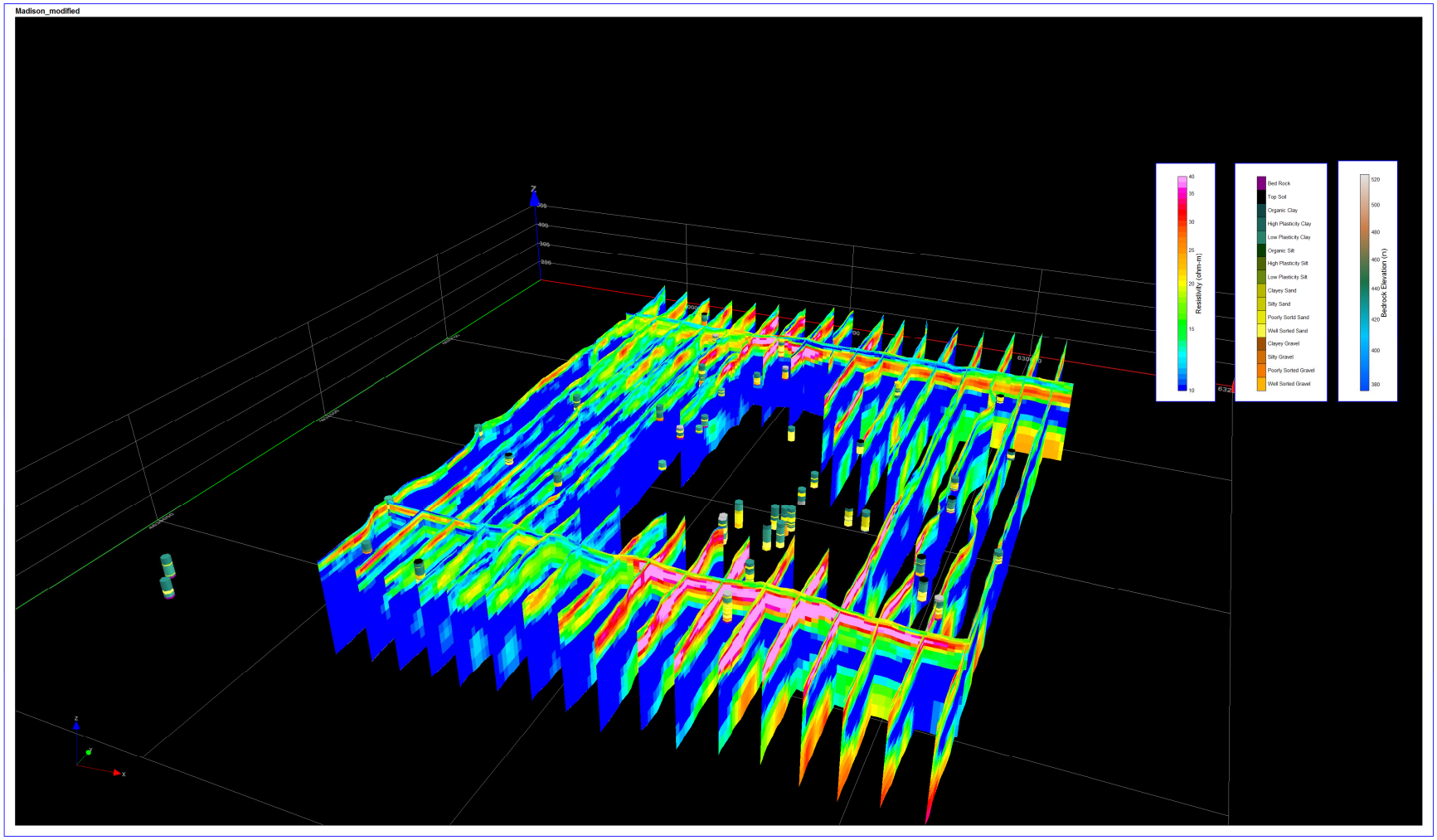


Figure A-2 – 3-D image displaying electromagnetic response of the subsurface along each flight line surrounding Madison (vertical exaggeration 3:1).

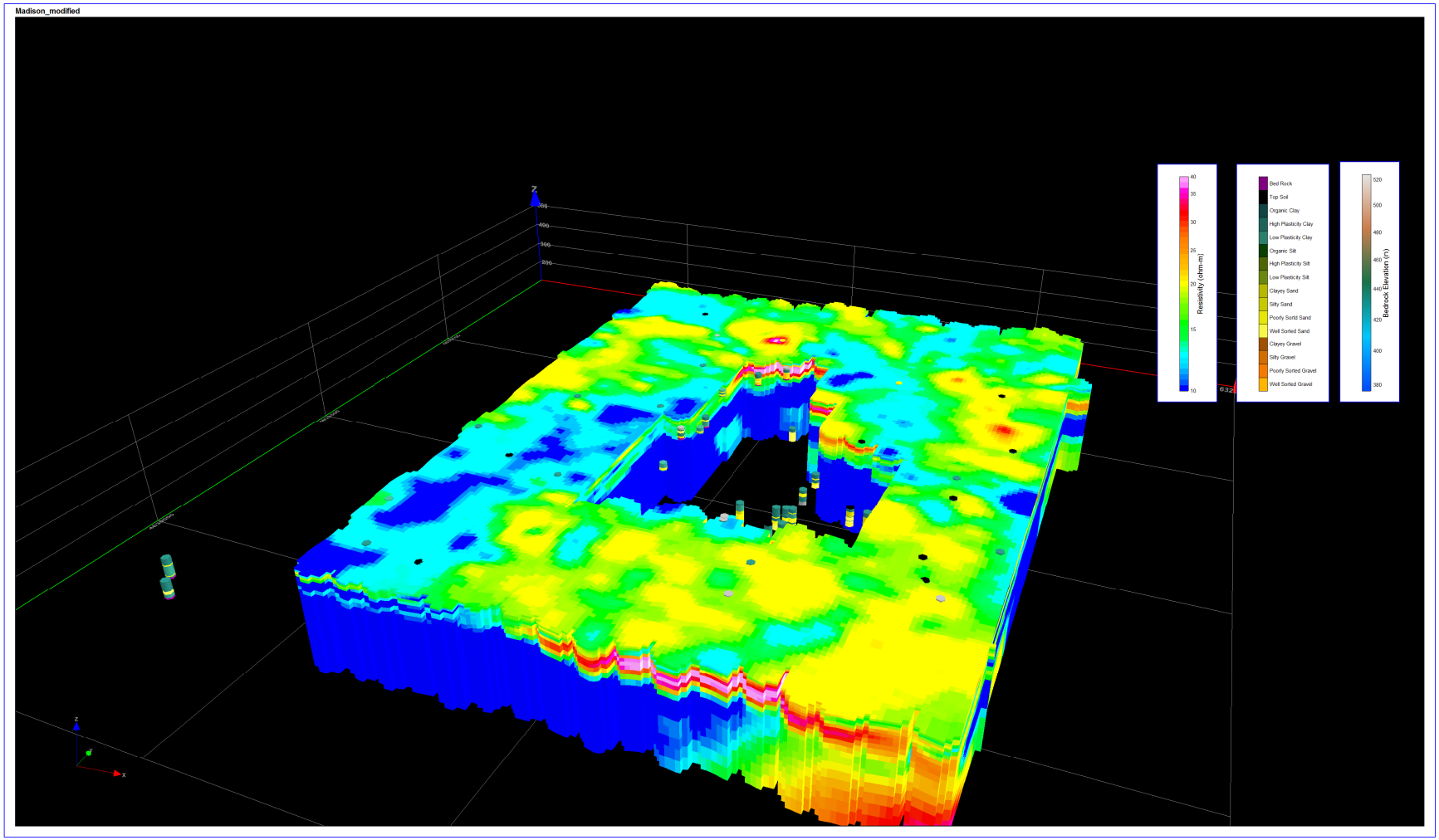


Figure A-3 – Image displaying the 3D resistivity model of the AEM survey (vertical exaggeration 3:1).

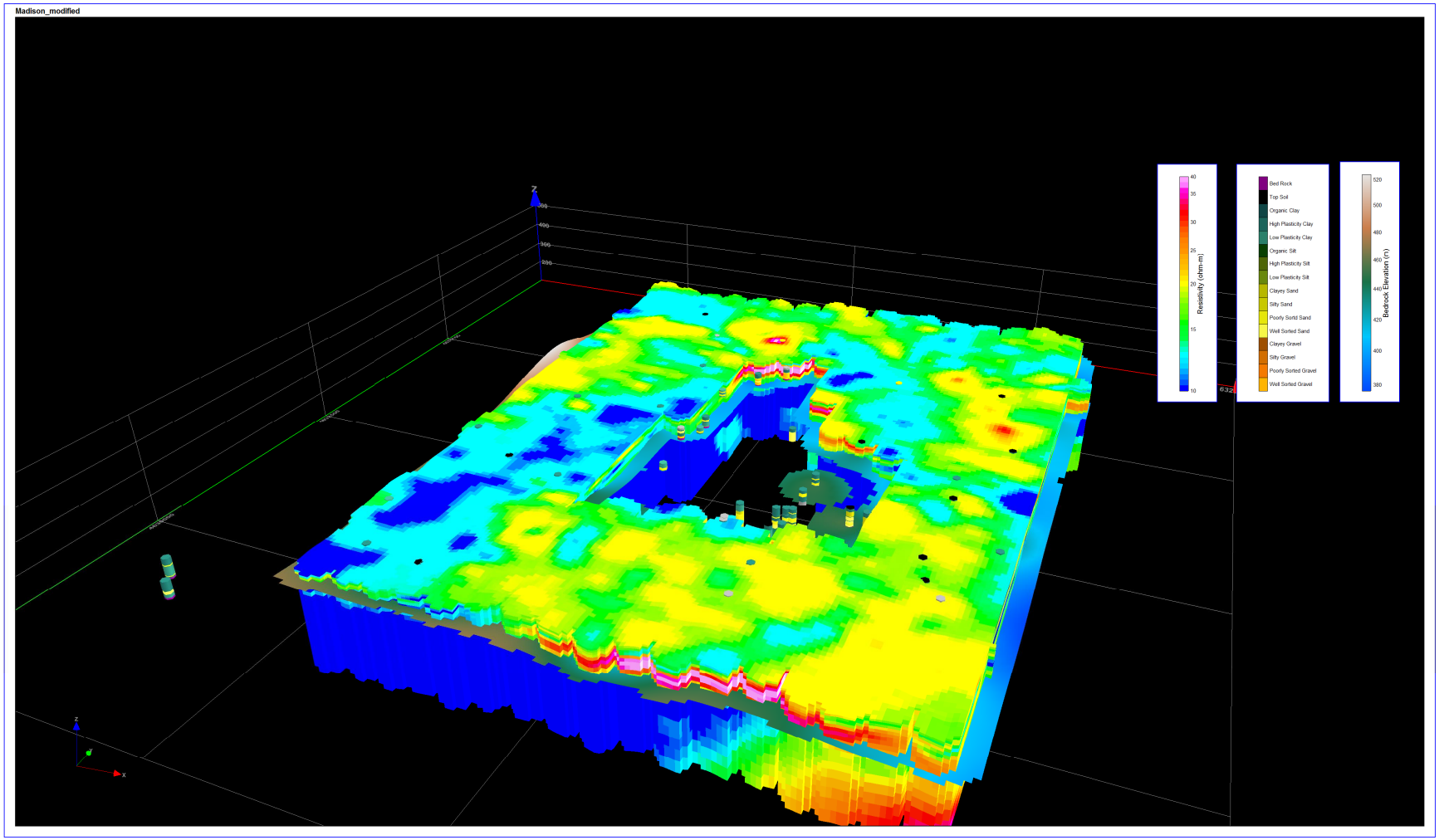


Figure A-4 – 3-D image displaying 3D resistivity model of the AEM survey contact between the Quaternary units and underlying bedrock demarcated as a horizontal layer (vertical exaggeration 3:1).

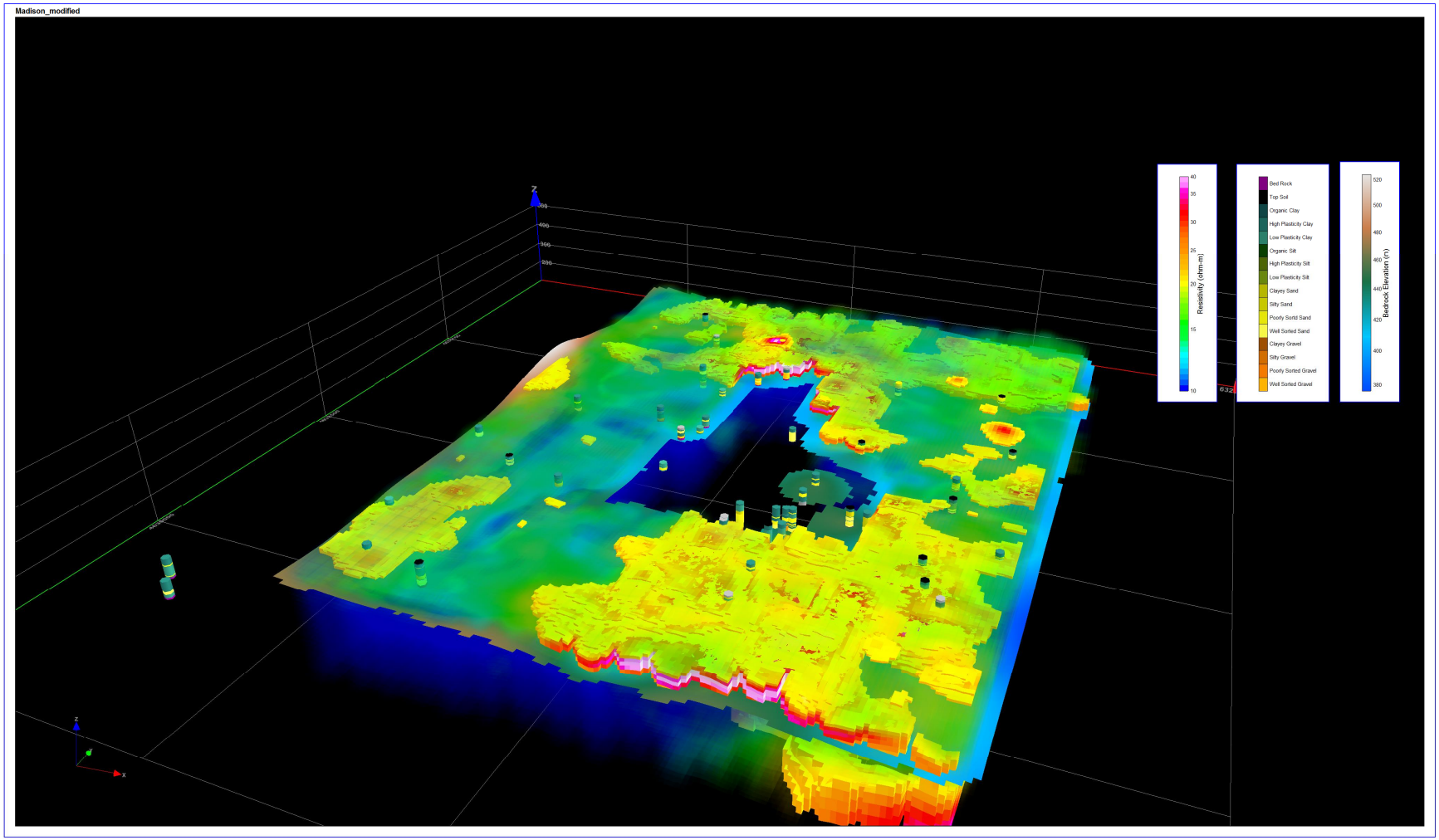


Figure A-5 – 3-D image of subsurface areas exhibiting resistivity values of 23 ohm-m or greater with the Quaternary unit-bedrock contact and depth of bedrock penetrated displayed (vertical exaggeration 3:1).

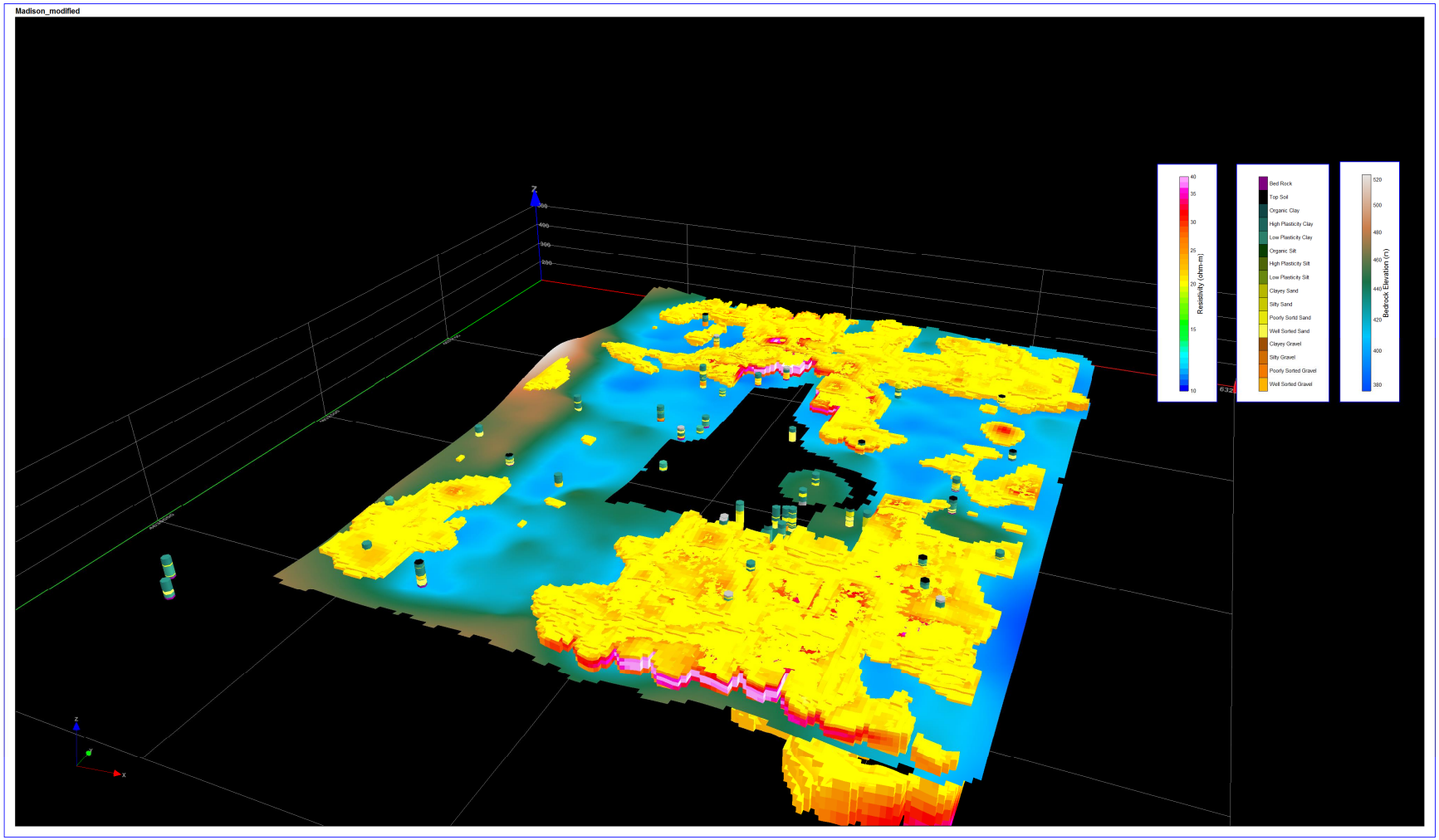


Figure A-6 – 3-D image of all Quaternary deposits and bedrock units with resistivity values of 23 ohm-m or greater (vertical exaggeration 3:1).

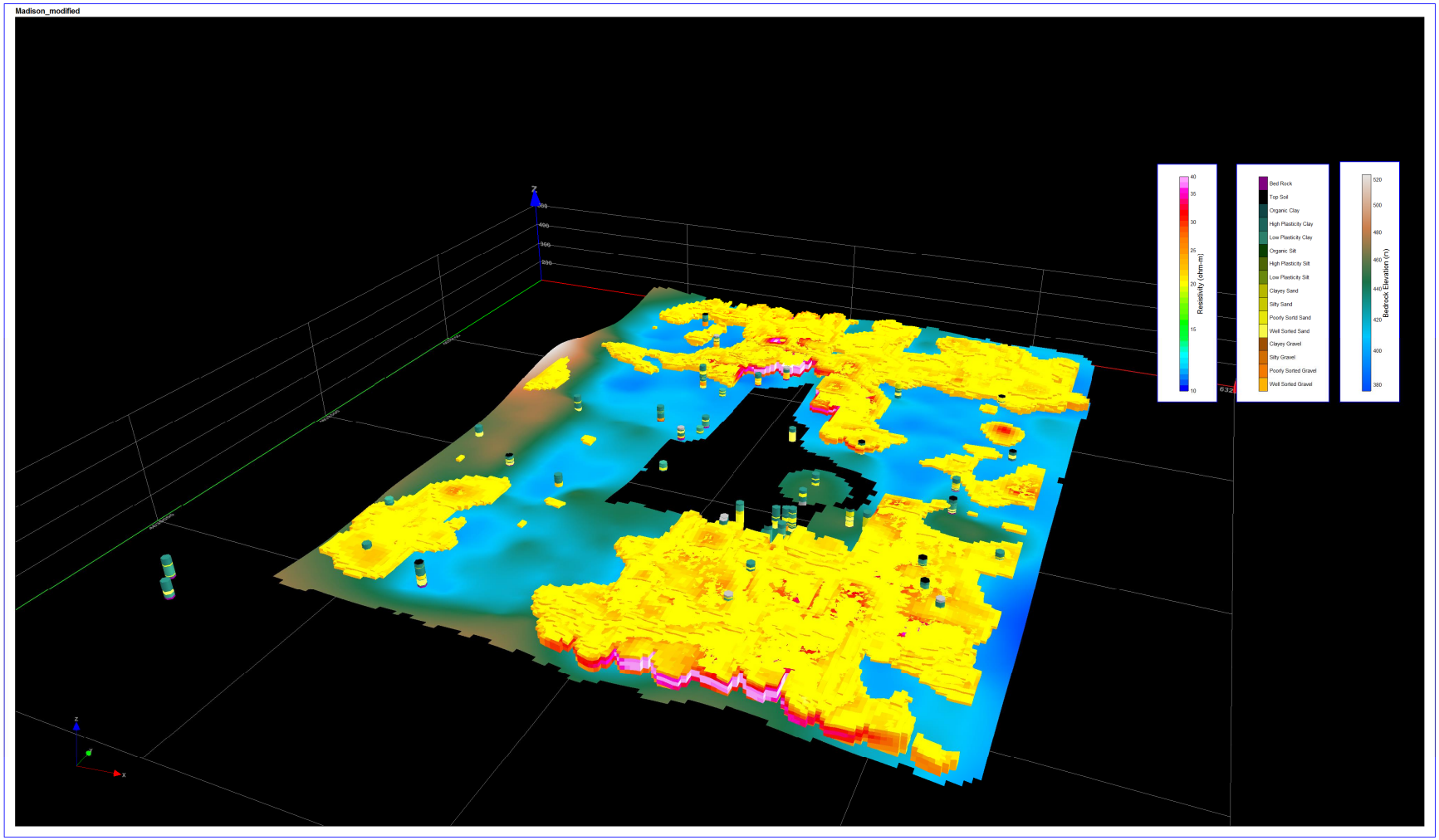


Figure A-7 – 3-D image of Quaternary deposits only with resistivity levels at 23 ohm-m or greater above the bedrock surface (vertical exaggeration 3:1).

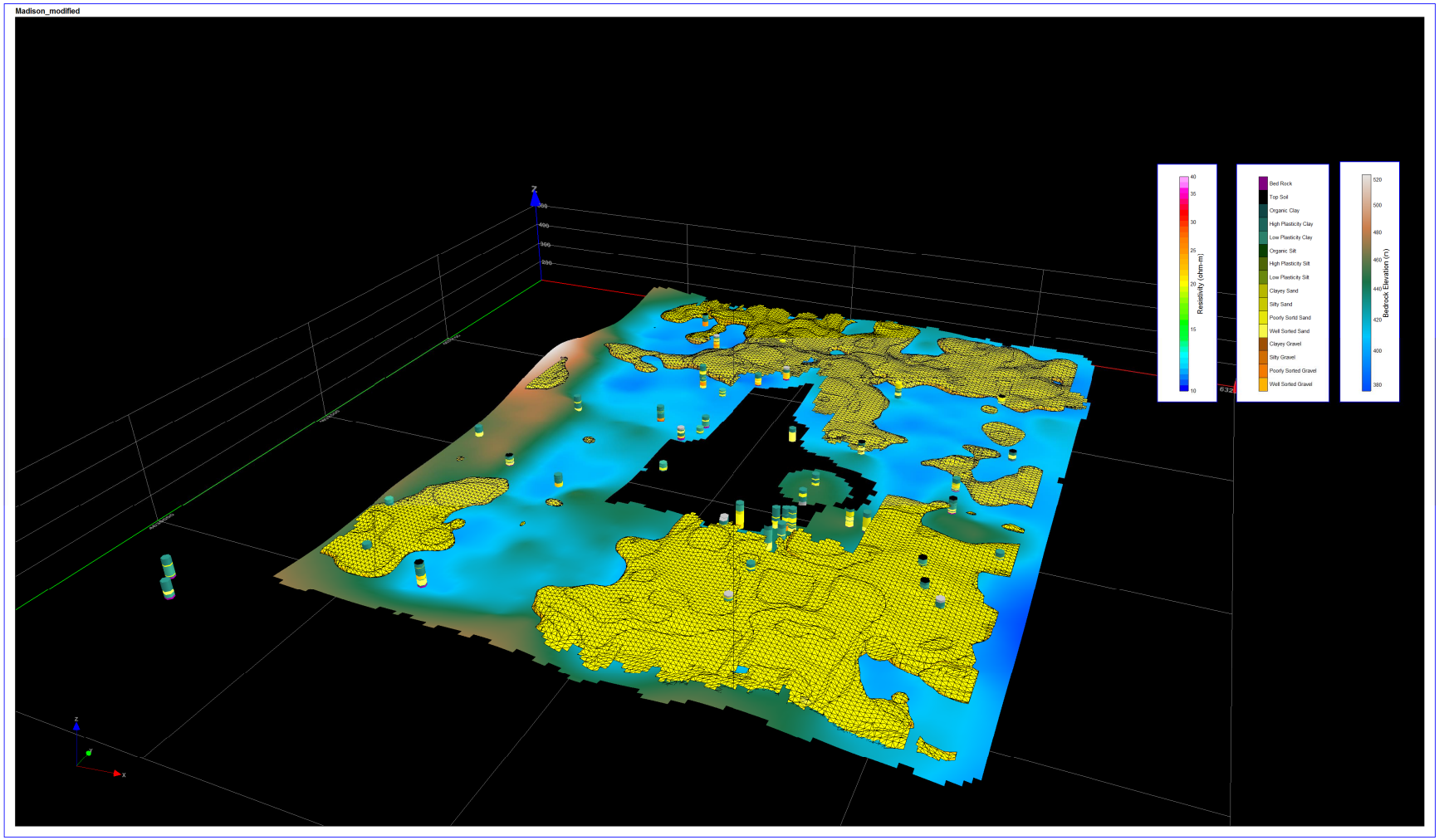


Figure A-8 – Distribution of the principal aquifer overlying the bedrock surface (vertical exaggeration 3:1).

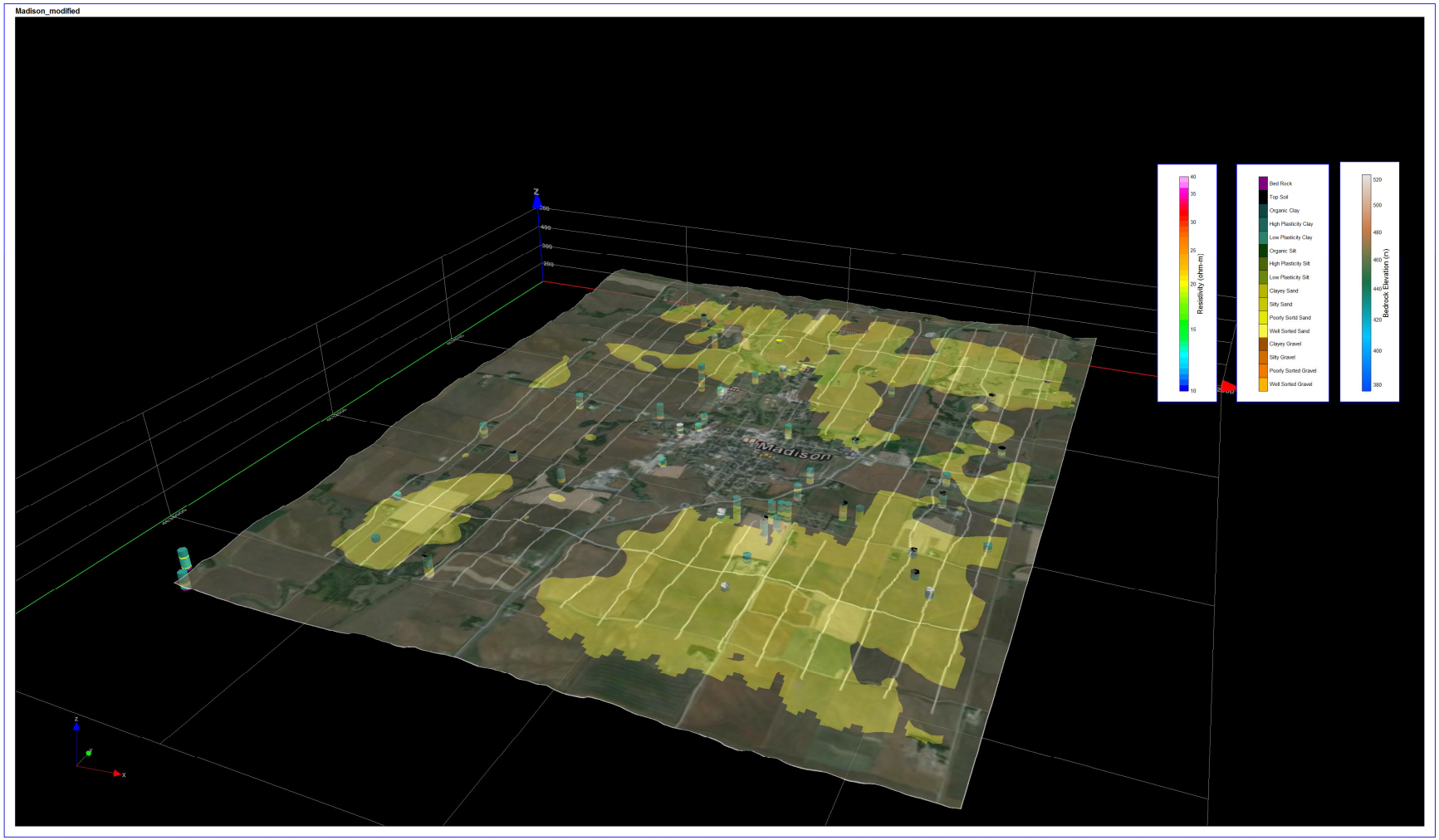


Figure A-9 – Distribution of the principal aquifer (as displayed in Figure A-8) with the AEM flight lines (gray lines) and land surface for reference of the aquifer location in relation to the city area (vertical exaggeration 3:1).

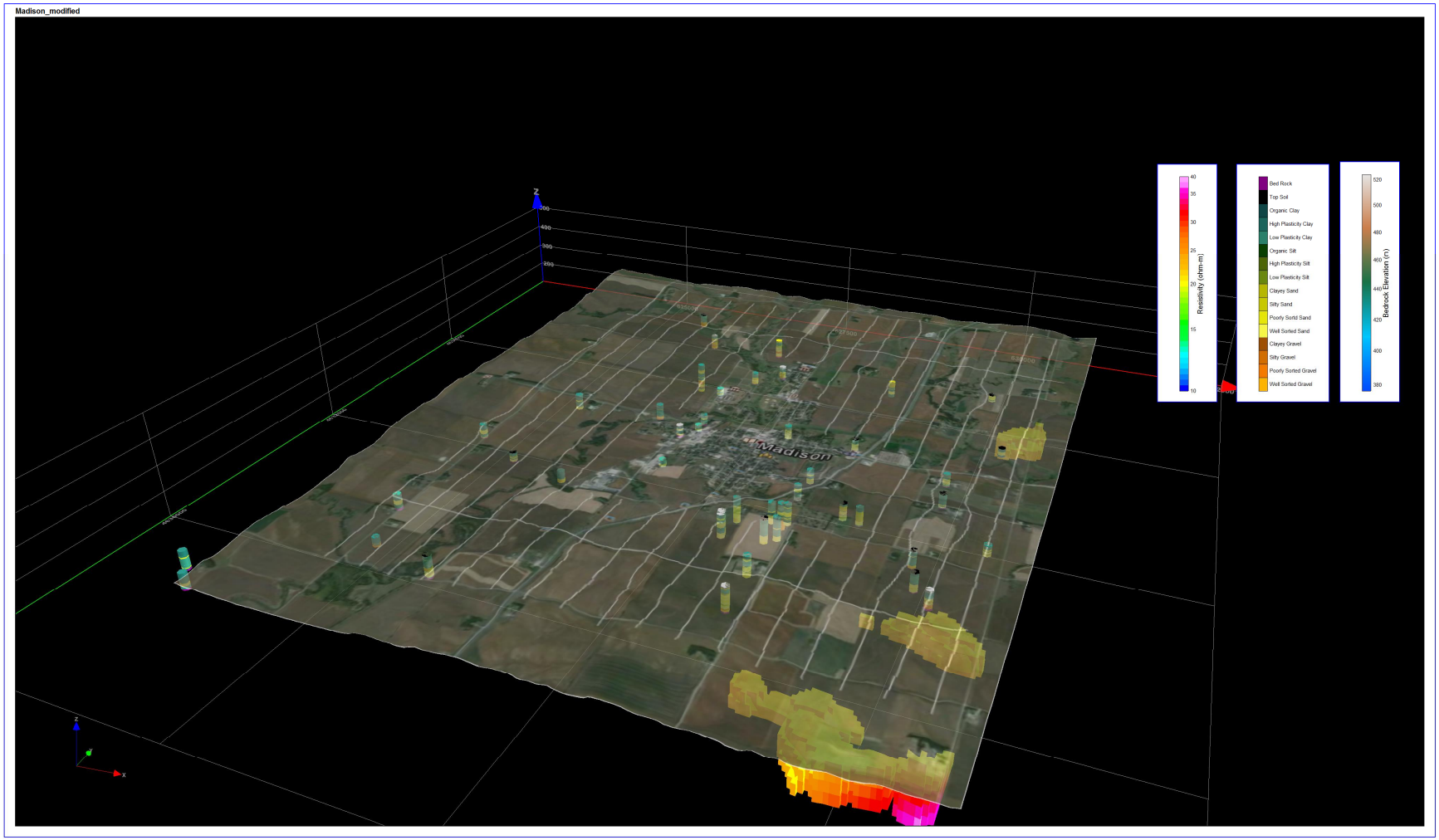


Figure A-10 – Location and distribution of bedrock units with resistivity levels of 23 ohm-m or greater underlying the project area with the AEM flight lines (gray lines) (vertical exaggeration 3:1).

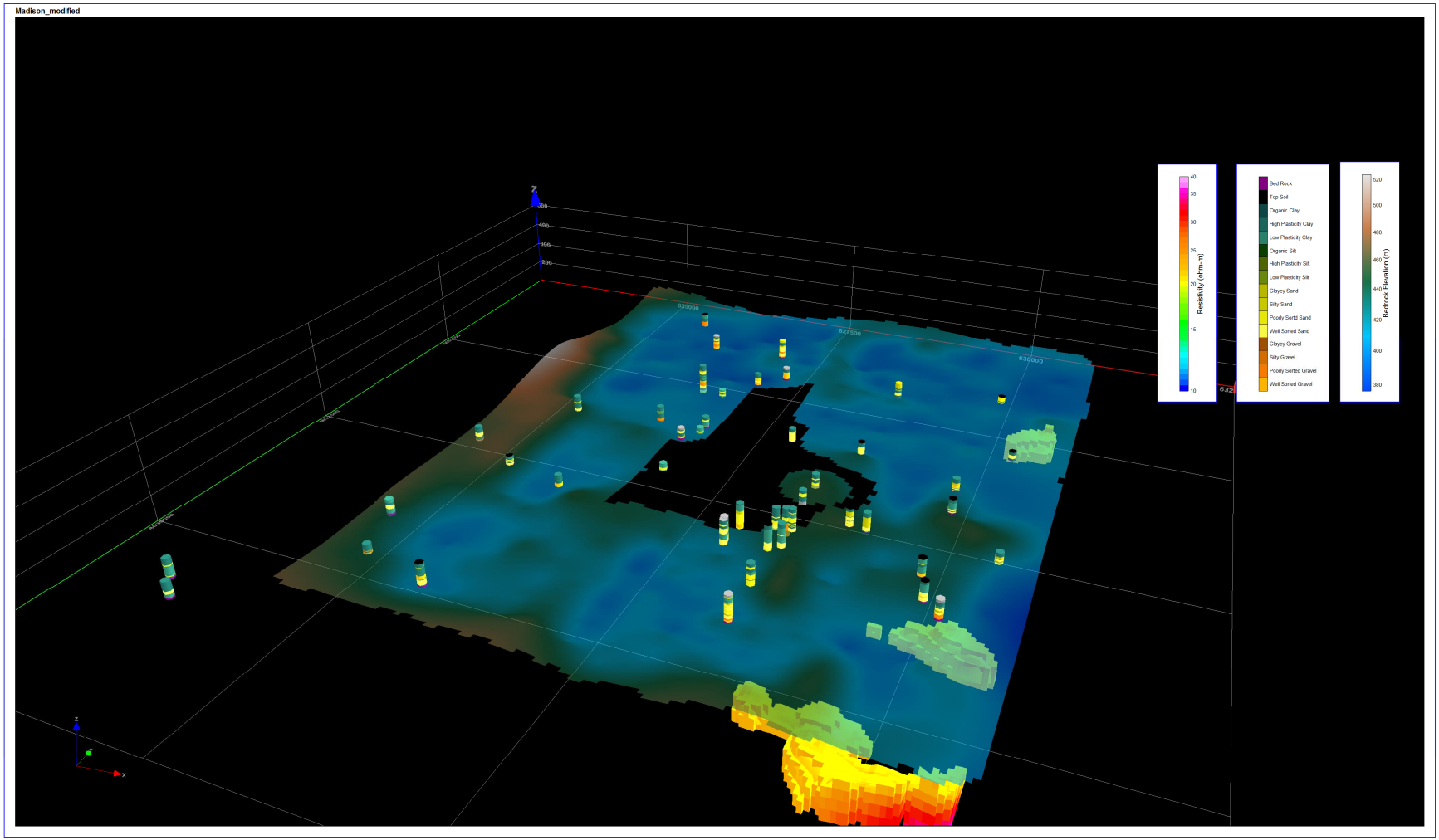


Figure A-11 – Location and distribution of bedrock units with resistivity levels at 23 ohm-m or greater underlying the bedrock surface. Also displayed are the borehole log locations with color-coded lithologies (vertical exaggeration 3:1).

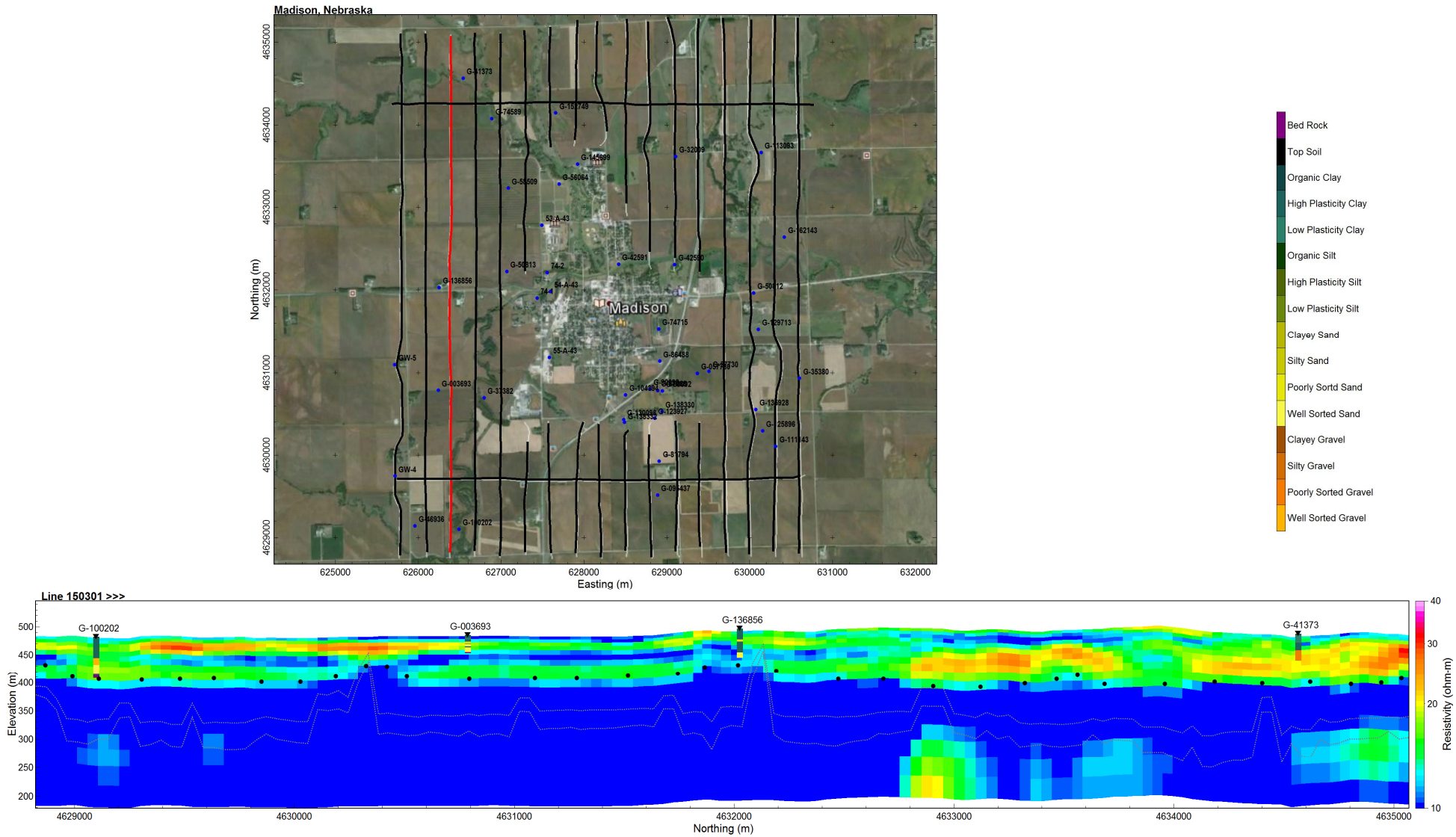


Figure A-12 –South to north cross section along the western side of the Madison survey area. AEM data collection locations (top map view), flight lines (black lines (red line is current viewed flight line)), and borehole locations (blue dots); resistivity model (lower plot) with boreholes and interpreted top of the Cretaceous bedrock (black dots) and depth of investigation upper and lower estimates (fine black dotted lines) (NAD83 UTM zone 14 N (meter), vertical datum is NAVD88 (meter)).

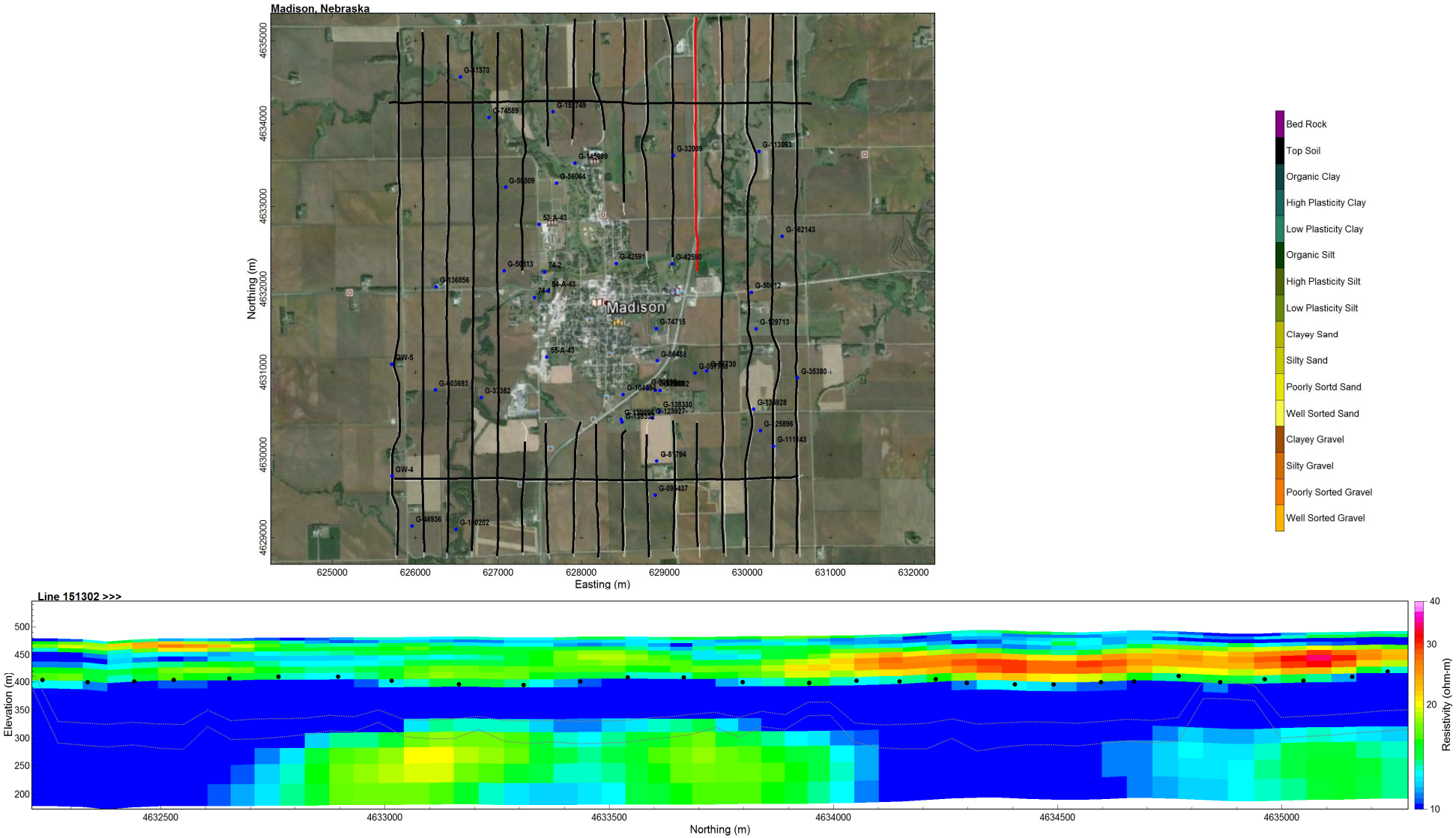


Figure A-13 – South to north cross section on the north east side of the Madison survey area. AEM data collection locations (top map view), flight lines (black lines (red line is current viewed flight line)), and borehole locations (blue dots); resistivity model (lower plot) with boreholes and interpreted top of the Cretaceous bedrock (black dots) and depth of investigation upper and lower estimates (fine black dotted lines) (NAD83 UTM zone 14 N (meter), vertical datum is NAVD88 (meter)).

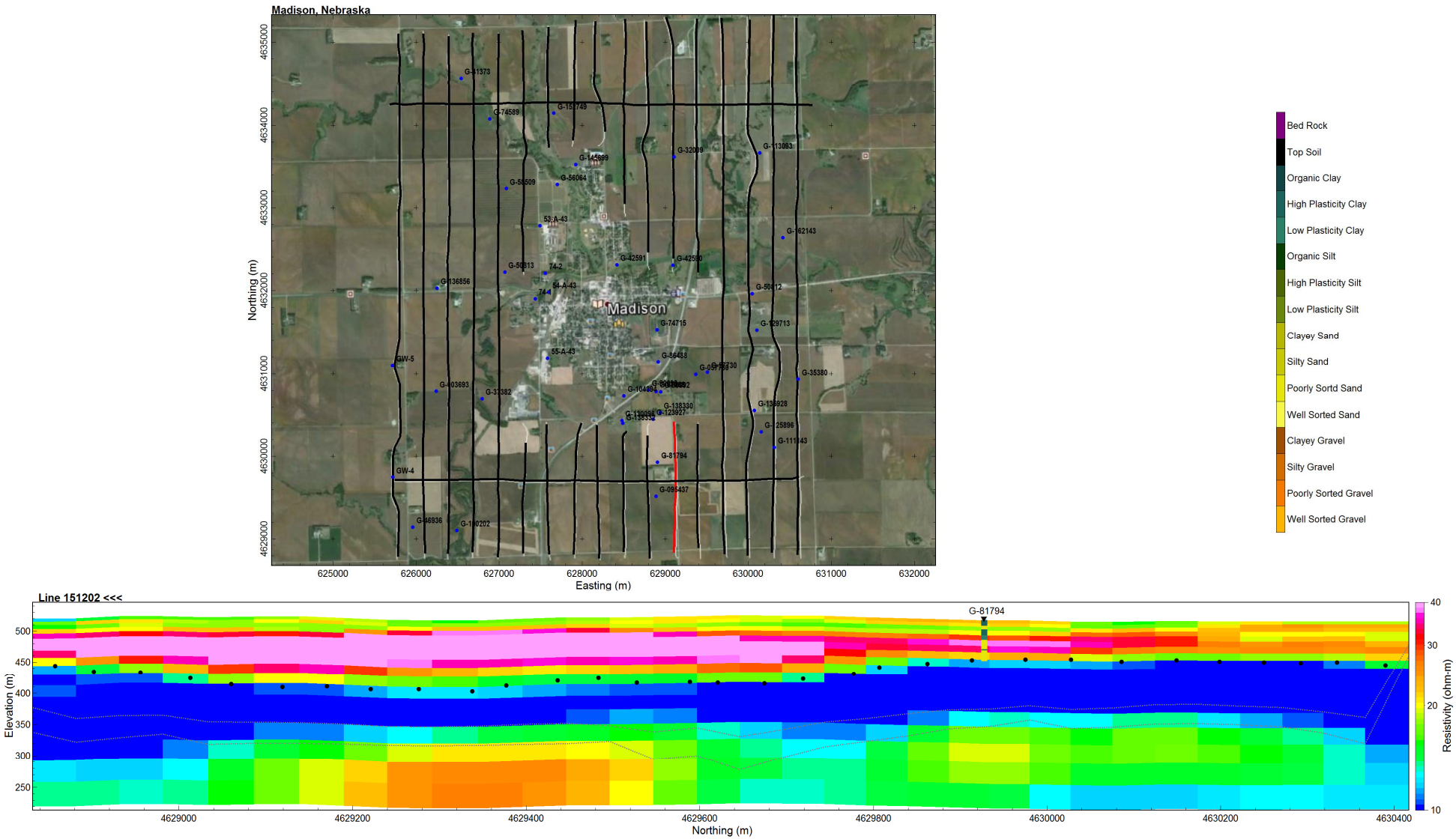


Figure A-14 – South to north cross section on the south east side of the Madison survey area. AEM data collection locations (top map view), flight lines (black lines *(*red line is current viewed flight line)), and borehole locations (blue dots); resistivity model (lower plot) with boreholes and interpreted top of the cretaceous bedrock (black dots) and depth of investigation upper and lower estimates (fine black dotted lines) (NAD83 UTM zone 14 N (meter), vertical datum is NAVD88 (meter)).

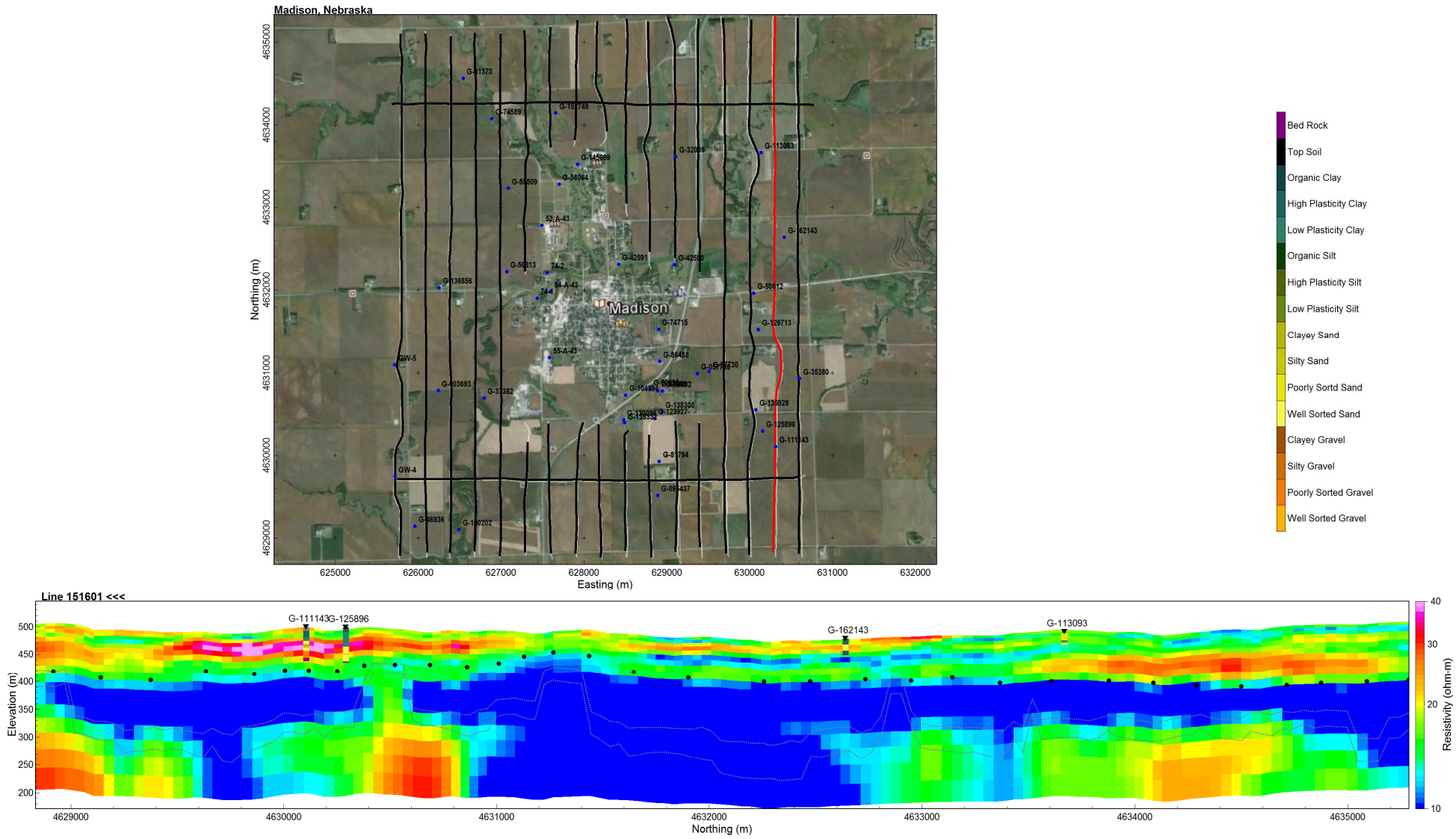


Figure A-15 – South to north cross section on the east side of the Madison survey area. AEM data collection locations (top map view), flight lines (black lines *(*red line is current viewed flight line)), and borehole locations (blue dots); resistivity model (lower plot) with boreholes and interpreted top of the Cretaceous bedrock (black dots) and depth of investigation upper and lower estimates (fine black dotted lines) (NAD83 UTM zone 14 N (meter), vertical datum is NAVD88 (meter)).

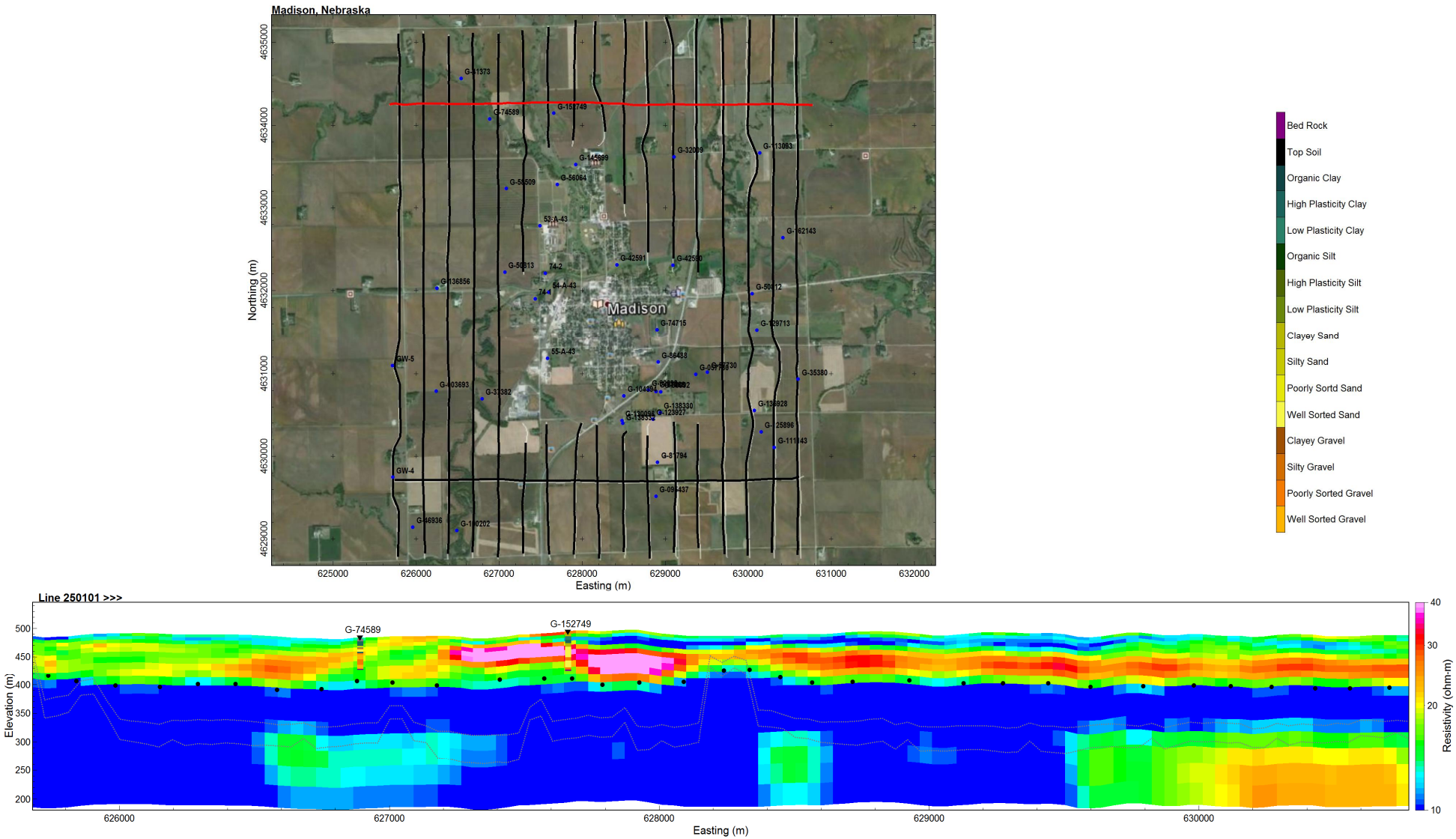


Figure A-16 – West to east cross section on the north of the Madison survey area. AEM data collection locations (top map view), flight lines (black lines (red line is current viewed flight line)), and borehole locations (blue dots); resistivity model (lower plot) with boreholes and interpreted top of the Cretaceous bedrock (black dots) and depth of investigation upper and lower estimates (fine black dotted lines) (NAD83 UTM zone 14 N (meter), vertical datum is NAVD88 (meter)).

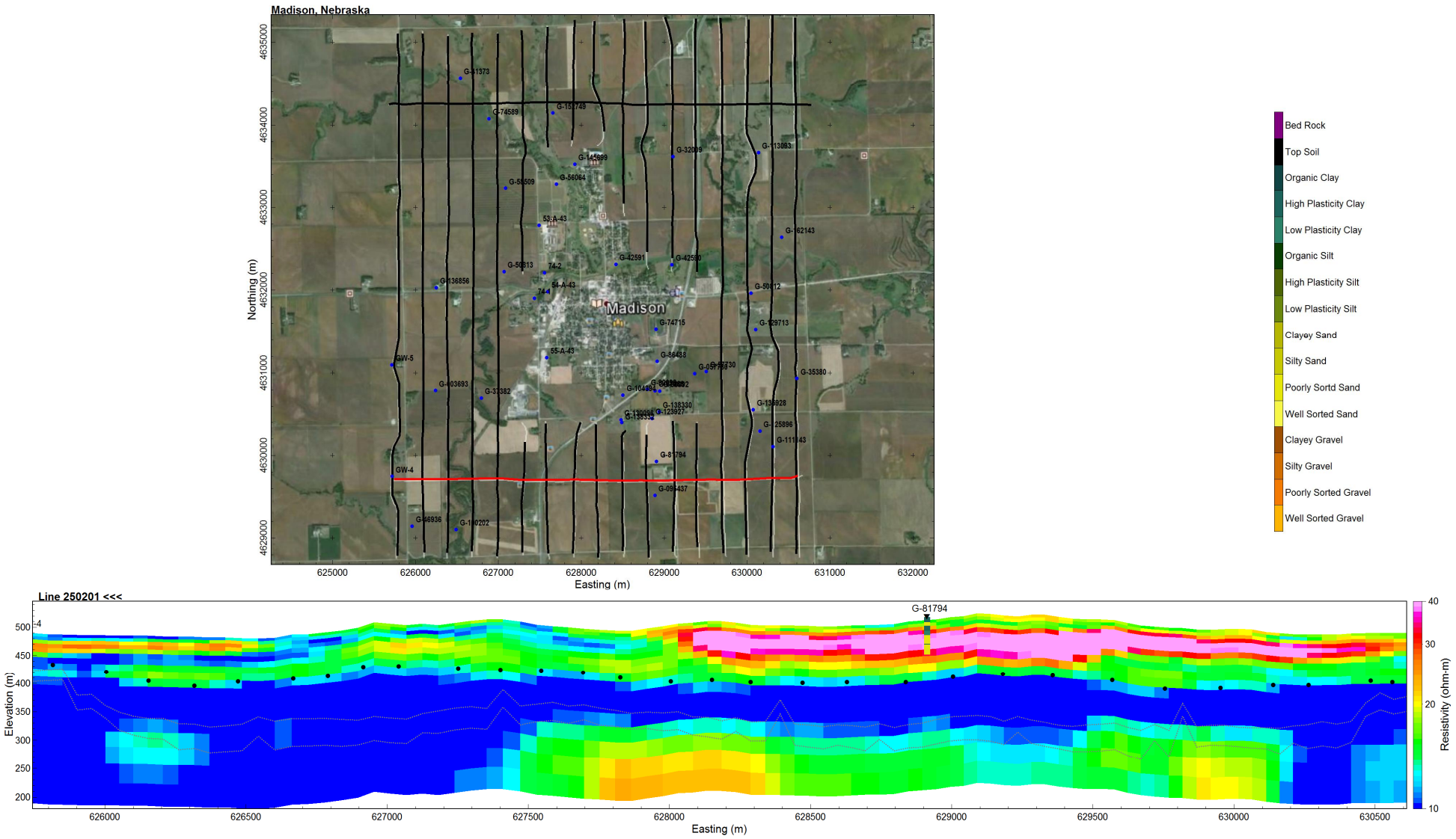


Figure A-17 – West to east cross section on the south of the Madison survey area. AEM data collection locations (top map view), flight lines (black lines (red line is current viewed flight line)), and borehole locations (blue dots); resistivity model (lower plot) with boreholes and interpreted top of the Cretaceous bedrock (black dots) and depth of investigation upper and lower estimates (fine black dotted lines) (NAD83 UTM zone 14 N (meter), vertical datum is NAVD88 (meter)).

Appendix 2 - Metadata

Metadata File Formats

The acquired and processed data are provided in the form of .XYZ files. The included files are:

- Madison_Inversion.xyz: results of inversion of AEM data, given in an array of modeled layers and earth resistivity
- Madison_AEM_MAG_data.xyz: results if AEM survey giving raw and processed magnetic and electromagnetic data

The data in these file are separated according to planned flight lines. The projection of the spatial data in the .XYZ files are given in UTM Zone 14N easting and northing (NAD83). The parameters within the both of the .XYZ files are listed in Tables A-1 and A-2.

Table A-1 - Parameters for metadata file Madison_Inversion.xyz

Parameter	Description	Unit
X	Easting NAD83 UTM Zone 14 North	Meter [m]
Y	Northing NAD83 UTM Zone 14 North	Meter [m]
TOPO	Helicopter recorded topography NAVD88	Meter [m]
ALT	Altitude recorded of SkyTEM sensor	Meter [m]
INVALT	Inverted Altitude	Meter [m]
DELTAALT	Difference from recorded and inverted altitude	Meter [m]
DEM_sample	The sampling of the USGS NED DEM	Meter [m]
RES[xx*]	Inverted layer resistivity value	Ohm-meter [Ým]
RES_STD[xx*]	Standard deviation of resistivity for inverted layer	Ohm-meter [Ým]
SIGNA[xx*]	Model versus data misfits for layer	N/A
TOP[xx*]	Inverted layer top	Meter [m]
Bottom[xx*]	Inverted layer bottom	Meter [m]
THK[xx*]	Inverted layer thickness	Meter [m]
DEP_BOT_STD[xx*]	Inverted layer standard deviations	N/A
DOI_UPPER	A numerical upper estimate of the depth of investigation	Meter [m]
DOI_Lower	A numerical lower estimate of the depth of investigation	Meter [m]
CHORDLEN	Distance between points	Meter [m]

***There are a total of 18 inverted layers, numbered 0-17.**

Table A-2 – Inversion layer top, bottom, and thickness

Layer Number	Top (meter)	Bottom (meter)	Thickness (meter)
0	0.0	-5.0	5.0
1	-5.0	-10.6	5.6
2	-10.6	-17.0	6.4
3	-17.0	-24.2	7.2
4	-24.2	-32.3	8.1
5	-32.3	-41.4	9.1
6	-41.4	-51.7	10.3
7	-51.7	-63.3	11.6
8	-63.3	-76.3	13.0
9	-76.3	-91.0	14.7
10	-91.0	-107.6	16.6
11	-107.6	-126.3	18.7
12	-126.3	-147.3	21.0
13	-147.3	-171.0	23.7
14	-171.0	-197.7	26.7
15	-197.7	-227.8	30.1
16	-227.8	-261.8	34.0
	-261.8	-300.0	38.2

Table A-3- Parameters for metadata file Madison_AEM_MAG_data.xyz

Parameter	Description	Unit
Alt	DGPS Altitude	Meters above sea level
AngleX	Angle (in flight direction)	Degrees
AngleY	Angle (perpendicular to flight direction)	Degrees
Bmag_Diur	Diurnal Variation - magnetic base station data	nanotesla [nT]
Bmag_raw	Total Magnetic Intensity ï raw magnetic data ï magnetic base station data	nanotesla [nT]
Curr_1	Current, High Moment	Amps
Curr_2	Current, Low Moment	Amps
Date	Date	yyyymmdd
DateTime	DateTime Format	Decimal days
DEM	Digital Elevation Model	Meters above sea level
E_NAD83	UTM Zone 14N (NAD83)	Meter [m]
Fid	Unique Fiducial Number	Seconds
Flight	Name of Flight	yyyymmdd.ff
GdSpeed	Ground Speed	Kilometers/hour [km/h]
Height	Filtered Height Measurement	Meters [m]
HM_X_G15[xx*]	Normalized High Moment X-RxCoil value	pV/(m^4*A)
HM_Z_G15[xx*]	Normalized High Moment Z-RxCoil value	pV/(m^4*A)
IGR_TMI	Calculated IGRF-10	nanotesla [nT]
Lat	Latitude, WGS84	Decimal Degrees
Line	Line Number	LLLLLL
LM_X_G10[xx*]	Normalized Low Moment X-RxCoil value	pV/(m^4*A)
LM_Z_G10[xx*]	Normalized Low Moment Z-RxCoil value	pV/(m^4*A)
Lon	Longitude, WGS84	Decimal Degrees
Mag_cor	Residual Magnetic Field ï corrected for diurnal, lag, heading and IGRF	nanotesla [nT]
Mag_fil	Filtered Magnetic Data	nanotesla [nT]
Mag_raw	Raw Magnetic Data ï total magnetic intensity - despiked	nanotesla [nT]
N_NAD83	UTM Zone 14N (NAD83)	Meter
PLNI_60Hz	Power Line Noise Intensity. Amplitude spectral density of the power line noise	N/A
RMF	Residual Magnetic Field ï IGRF removed ï final corrected and leveled magnetic data	nanotesla [nT]
Time	Time	hhmmss.sss
TMI	Total Magnetic Intensity ï final corrected and leveled magnetic data; IGRF recalculated	nanotesla [nT]

***High Moment and low moment measurement channels correspond with time gate numbers listed in Table A-3.**

All recorded data are time stamped in order to correlate independent data sets. The time stamps are in Coordinated Universal Time/Greenwich Mean Time (UTC/GMT) which is a +6 hour difference from Central Standard Time. Time stamps are one of the two following formats.

- Date and time defined as: yyyy/mm/dd hh:mm:ss.sss
- Date and time values defined as the number of days since 1900/01/01 and seconds of the day: ddddd.sssssssss (decimal days).

Time Gates

There are a total of 38 time gates. Table A-4 presents the gate number, the gate center, gate width and a comment concerning time gate usage.

Table A-4 - Time Gate Information

Gate No.	Gate Center (µs)	Gate Width (µs)	Comment	Gate No.	Gate Center (µs)	Gate Width (µs)	Comment
0	-0.385	1.57	Not Used	19	172.115	38.57	Low and High Moment
1	1.615	1.57	Not Used	20	216.115	48.57	Low and High Moment
2	3.615	1.57	Not Used	21	271.615	61.57	Low and High Moment
3	5.615	1.57	Not Used	22	342.115	78.57	Low and High Moment
4	7.615	1.57	Not Used	23	431.615	99.57	Low and High Moment
5	9.615	1.57	Low Moment Only	24	544.615	125.57	Low and High Moment
6	11.615	1.57	Low Moment Only	25	687.115	158.57	Low and High Moment
7	13.615	1.57	Low Moment Only	26	867.115	200.57	Low and High Moment
8	16.115	2.57	Low Moment Only	27	1094.615	253.57	Low and High Moment
9	19.615	3.57	Low Moment Only	28	1382.115	320.57	Low and High Moment
10	24.115	4.57	Low Moment Only	29	1745.115	404.57	High Moment Only
11	29.615	5.57	Low Moment Only	30	2203.115	510.57	High Moment Only
12	36.615	5.57	Low Moment Only	31	2781.615	645.57	High Moment Only
13	45.615	9.57	Low Moment Only	32	3512.615	815.57	High Moment Only
14	56.615	11.57	Low and High Moment	33	4436.115	1030.57	High Moment Only
15	70.115	14.57	Low and High Moment	34	5602.615	1301.57	High Moment Only
16	87.115	18.57	Low and High Moment	35	7075.615	1643.57	High Moment Only
17	109.115	24.57	Low and High Moment	36	8936.115	2076.57	High Moment Only
18	137.115	30.57	Low and High Moment	37	11286.115	2622.57	High Moment Only

Appendix 3 - Ancillary Data

Appendix 3- Ancillary Data

Instrumentation

Instrumentation of the SkyTEM includes a time domain electromagnetic (TDEM) system (one transmitter [Tx] and two receivers [Rx] positioned orthogonally in line with the x and z axes) and a magnetometer as well as data acquisition systems for both of these instruments. The SkyTEM also includes two each of laser altimeters, inclinometers/tilt meters and DGPS receivers. Positional data from the frame mounted DGPS receivers are recorded by the TDEM data acquisition system. The magnetometer includes a third DGPS receiver, this positional data is recorded by the magnetometer data acquisition system. Figure A-18 gives a simple illustration of the SkyTEM frame and instrument locations, the image is viewed along the +z axis looking at the horizontal x-y plane. The axes for the image are labelled with distance in meters. The square symbols denote the locations of the altimeters, the triangles denote the DGPS positions and the circles denote the inclinometers. The magnetometer is located on a boom off the front of the frame (right side of image, arrow indicates +x direction as well as direction of flight). The TDEM Tx coil is located around the octagonal frame and the Rx Coils (x and z) are located at the back of the frame, left side of image).

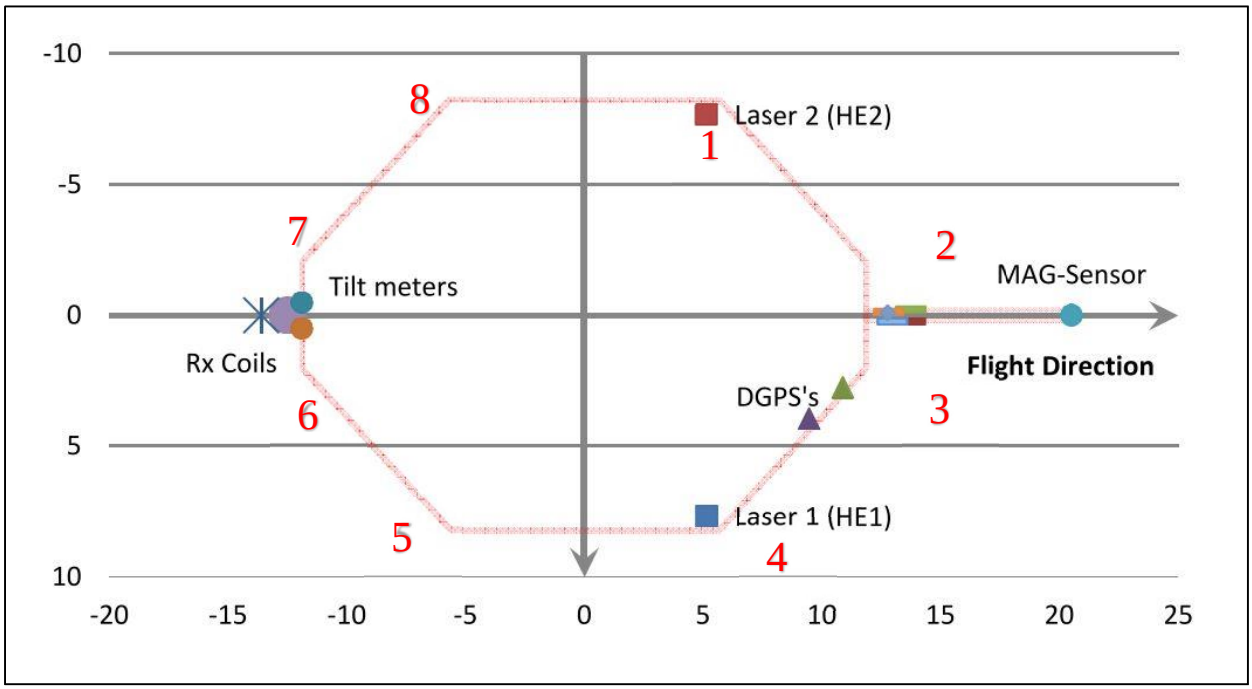


Figure A-18 - Simple illustration of SkyTEM frame including instrument locations.

The coordinate system used defines the +x direction as the direction of flight, the +y direction is defined 90° to the right and the +z direction is downward. The center of the transmitter loop, mounted to the octagonal SkyTEM frame is used as the origin when considering instrumentation positions. The Table A-5lists the positions of the instruments (in meters) and Table A-6 lists the corners of the transmitter loop (labeled in red numbers in Figure A-18).

Table A-5 - Instrumentation positions on SkyTEM frame.

Instrument	DGPS 1	DGPS 2	Inclinometer 1	Inclinometer 2	Altimeter HE1	Altimeter HE2	X Rx Coil	Z Rx Coil
X	9.90	9.90	-11.65	-11.65	5.13	5.13	-13.60	-12.50
Y	2.69	3.66	0.50	0.50	7.85	-7.79	0.00	0.00
Z	-0.28	-0.28	-0.37	-0.37	-0.13	-0.13	-0.02	-2.21

Table A-6 - Corner positions of Tx loop on SkyTEM frame.

TX Corners	1	2	3	4	5	6	7	8
X	5.68	11.87	11.87	5.68	-5.68	-11.87	-11.87	-5.68
Y	8.22	2.03	-2.03	-8.22	-8.22	-2.03	2.03	8.22

DGPS and magnetometer base stations were placed at the locations listed in Table A-7. The geodetic reference used is NAD83; the unit of measurement is in meters.

Table A-7 - Locations of base station instruments.

Instrument	UTM X, easting	UTM Y, northing	UTM Zone	Elevation
DGPS Base Station	645119	4618553	14N	467.03
Magnetometer Base Station	644406	4619213	14N	505